In compliance with the
Canadian Privacy Legislation
some supporting forms
may have been removed from
this dissertation.

While these forms may be included
in the document page count,
their removal does not represent
any loss of content from the dissertation.

University of Alberta

Open- and Closed-Loop Identification of Multirate Systems

by

Jiandong Wang

A thesis submitted to the Faculty of Graduate Studies and Research in partial fulfillment of the requirements for the degree of **Master of Science**.

Department of Electrical and Computer Engineering

Edmonton, Alberta
Fall 2003

National Library of Canada
Acquisitions and Bibliographic Services
395 Wellington Street
Ottawa ON K1A 0N4
Canada

Bibliothèque nationale du Canada
Acquisisitons et services bibliographiques
395, rue Wellington
Ottawa ON K1A 0N4
Canada

Your file Votre référence
ISBN: 0-612-87908-9
Our file Notre référence
ISBN: 0-612-87908-9

The author has granted a non-exclusive licence allowing the National Library of Canada to reproduce, loan, distribute or sell copies of this thesis in microform, paper or electronic formats.

The author retains ownership of the copyright in this thesis. Neither the thesis nor substantial extracts from it may be printed or otherwise reproduced without the author's permission.

L'auteur a accordé une licence non exclusive permettant à la Bibliothèque nationale du Canada de reproduire, prêter, distribuer ou vendre des copies de cette thèse sous la forme de microfiche/film, de reproduction sur papier ou sur format électronique.

L'auteur conserve la propriété du droit d'auteur qui protège cette thèse. Ni la thèse ni des extraits substantiels de celle-ci ne doivent être imprimés ou aturement reproduits sans son autorisation.

Canada

University of Alberta

Library Release Form

Name of Author: Jiandong Wang

Title of Thesis: Open- and Closed-Loop Identification of Multirate Systems

Degree: Master of Science

Year this Degree Granted: 2003

Permission is hereby granted to the University of Alberta Library to reproduce single copies of this thesis and to lend or sell such copies for private, scholarly or scientific research purposes only.

The author reserves all other publication and other rights in association with the copyright in the thesis, and except as herein before provided, neither the thesis nor any substantial portion thereof may be printed or otherwise reproduced in any material form whatever without the author's prior written permission.

Date: June 9th, 2003

University of Alberta

Faculty of Graduate Studies and Research

The undersigned certify that they have read, and recommend to the Faculty of Graduate Studies and Research for acceptance, a thesis entitled **Open- and Closed-Loop Identification of Multirate Systems** submitted by Jiandong Wang in partial fulfillment of the requirements for the degree of **Master of Science**.

Dr. Edward S. Meadows

Date: June 4, 2003

Abstract

This thesis consists of two parts. The first part (Chapter 1 to Chapter 5) studies identification of a general multirate sampled-data system. Using the lifting technique, we associate the multirate system with an equivalent linear time-invariant system, from which a fast-rate discrete-time system is extracted. Uniqueness of the fast-rate system, controllability and observability of the lifted system, approaches of extracting fast-rate systems and other related issues are discussed in a complete manner. The effectiveness is demonstrated through simulation and real-time implementation.

The second part (Chapter 6) addresses a challenge: Is a closed-loop system without external excitation identifiable? The so-called fast-sampling direct approach provides a positive answer. It removes a traditional restrictive identifiability condition for linear output feedback closed-loop systems, i.e., an external persistently exciting test signal is not required. Identifiability is analyzed using the lifting technique, the bifrequency maps and bispectra concepts. The proposed approach is evaluated by simulation.

Dedication

This body of work is dedicated to Qingkun whose support and encouragement have transformed my life. She is the source of motivation and inspiration. "You are a person who may not be the best at the very beginning, but is capable of learning with all heart and ending with great achievements.". Her comment makes me feel flattered, but at the same time, I am always encouraged.

Acknowledgements

I would like to take the opportunity to thank all the people who have helped me to complete this thesis.

First of all, an incredible debt of gratitude is owed to my supervisors, Dr. Tongwen Chen and Dr. Biao Huang, for their outstanding guidance and support all the way. Their encouragement, enthusiasm and friendship have been vital in the creation of this thesis and the research it contains. Working with them has enriched my knowledge and broaden my horizons beyond measure. I am especially thankful to Dr. Chen for his funding and giving me an opportunity to study at UofA.

I would like to thank the other members of my committee for their input and interest: Dr. Alan Lynch and Dr. Edward S. Meadows. I am grateful to other professors in the Systems Group and in the Computer Process Control Group, Dr. Horacio J. Marquez, Dr. Qing Zhao, Dr. Fraser Forbes and Dr. Sirish L. Shah, for their assistance and help.

I would also like to thank my labmates, Dejan, Donglin, Feng, Guofeng, Jie, Yang, Zhihan and postdoctoral fellows, Dr. Ding, Dr. Sun, Dr. Tan, Dr. Xu, for the friendship, company and entertainment they provided. Discussions with them have often helped me a lot in my research.

Finally, I would like to thank my parents and my sister for their sacrifice, constant support and inspiration, and for encouraging me to pursue higher studies.

Contents

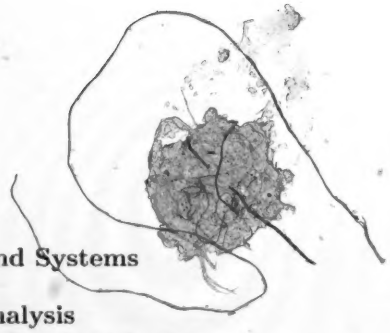

1 Introduction 1

2 Lifting Signals and Systems 4

3 Identifiability Analysis 9
- 3.1 Uniqueness of Fast-Rate Systems . . . 9
- 3.2 Controllability and Observability of Lifted Systems . . . 10

4 Fast-Rate Model Computation 13
- 4.1 Time-Domain Approach . . . 13
- 4.2 Frequency-Domain Approach . . . 16
- 4.3 Examples . . . 18

5 Noise Model and MIMO MRSD Systems 22
- 5.1 Noise Model Discussion . . . 22
- 5.2 Extension into MIMO MRSD Systems . . . 24

6 Fast-Sampling Direct Identification of Closed-Loop Systems 28
- 6.1 Introduction . . . 28
- 6.2 Preliminary . . . 30
- 6.3 A Basic Idea . . . 32
- 6.4 Lifting Technique in the Closed-Loop System . . . 33
- 6.5 Statistical Analysis of the Prediction Error . . . 37
- 6.6 Bifrequency Maps and Bispectra . . . 40
  - 6.6.1 Bifrequency Maps . . . 40
  - 6.6.2 Bispectra . . . 44
  - 6.6.3 Transformation of Bispectra by Linear Systems . . . 46
- 6.7 Identifiability Analysis Using Bispectra . . . 48
- 6.8 Examples and Analysis . . . 51

7 Conclusion 59

Bibliography 61

Appendix A 65

Appendix B 67

List of Figures

1.1 A SISO multirate sampled-data system 1

2.1 A SISO noise-free MRSD system 4
2.2 The lifted multirate sampled-data system 5

4.1 Simulation diagram of a SISO MRSD system 19
4.2 Step responses of the actual system (solid) and the estimated fast-rate models by the controllability and observability approach (dash), the matrix roots approach (dotted), and the frequency-domain approach (circle) 20
4.3 Comparison of the measured water level (solid) and the estimated water level (dotted) 21

5.1 Block diagram of a SISO MRSD system with a noise system 23
5.2 The lifted SISO MRSD system with a noise system 23
5.3 A general MIMO MRSD system 24
5.4 Simulation diagram of an MISO MRSD system 25
5.5 The lifted MISO MRSD system 26
5.6 Step responses and Bode plots of actual system G_{d1} from u_1 to y (solid) and the estimated model $\hat{G}_{d1}$ (dotted) 27
5.7 Step responses and Bode plots of actual system G_{d2} from u_2 to y (solid) and the estimated model $\hat{G}_{d2}$ (dotted) 27

6.1 Block diagram of a typical closed-loop system 29
6.2 Traditional direct approach in a closed-loop system without external excitation 32
6.3 A closed-loop system with multirate blocks 33
6.4 A lifted closed-loop system No.1 34
6.5 A lifted closed-loop system No.2 35
6.6 A lifted closed-loop system No.3 36
6.7 Filter bank representation of general LPTV systems 41
6.8 Bifrequency maps for $P = 2$ 45
6.9 Projection of bifrequency maps on the ω'-ω plane: (a) $P = 1$, (b) $P = 2$, (c) $P = 3$, (d) $P = 4$ 45
6.10 Schematic illustration of transformation of bispectra by linear systems. . . 46
6.11 Projection of bispectrum and cross bispectra of signals in a closed-loop system: (a) Φ_u, (b) Φ_{ue}, (c) Φ_{eu} 48
6.12 Block diagram of a closed-loop system without external excitation 52
6.13 Bode plots of G_0 (solid) and G_θ obtained by the fast-sampling direct approach (dotted) and by the traditional direct approach (dashdot) 53

6.14 Bode plots of N_0 (solid) and N_θ obtained by the fast-sampling direct approach (dotted) and by the traditional direct approach (dashdot) 53
6.15 Step responses and Bode plots of G_0 (solid) and G_θ obtained by the fast-sampling direct approach (dotted) 54
6.16 Step responses and Bode plots of N_0 (solid) and N_θ obtained by the fast-sampling direct approach (dotted) 54

Chapter 1

Introduction

The term Multirate Systems or Multirate Sampled-Data (MRSD) Systems describes a common phenomena existing in the industry that different variables are sampled at different rates for some reasons [4, 8], e.g., a high-purity distillation column [25], a bioreactor [16] and CCR octane quality control [28]. Figure 1.1 depicts a single-input and single-output (SISO) MRSD system, where G_c is a continuous-time linear time-invariant (LTI) and causal system with or without a time delay; H_{mh} is a zero-order hold with an updating period mh and S_{nh} is a sampler with period nh. Here m and n are different positive integers,[1] and h is a positive real number called the base period. Discrete-time signals u and y are the system input and output respectively; a continuous-time signal v_c is the unmeasured disturbance. Essentially, it is a linear periodically time-varying (LPTV) system [23], to which many system identification algorithms cannot apply directly.

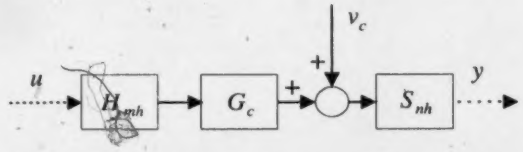

Figure 1.1: A SISO multirate sampled-data system

Under such a framework, Lu and Fisher [32, 33] used an output error method and a least-squares method to estimate intersample outputs based on the fast-sampled inputs and slow-sampled outputs. Doi and Phillips [11] developed multiple parametric models for the multirate systems using least-squares algorithms proposed by Lu and Fisher [33]. Verhaegen and Yu [43] extended a Multivariable Output Error State Space (MOESP) class of algorithms to identify p subsystems of a p-periodic LPTV process. Gudi *et al.* [16] generated frequent estimates of the primary output based on the secondary outputs and the

[1] There exist MRSD systems whose sampling periods do not have integral ratios [19].

regular measurement of inputs by an adaptive inferential strategy. Li *et al.* [27] identified a fast single-rate model with period mh from multirate input and output data[2], with an assumption that $m < n$. This work motivates us: Could we do better?

Doing better implies two things: first, a fast-rate model with period h instead of mh will be identified; second, a general MRSD system is treated without the assumption $m < n$. Note that our objective includes that of Li *et al.* [27], since a model with period mh is readily obtained from a model with period h. The improvement is significant: technically, we need to use additional conditions such as observability of lifted models and coprimeness of the integers m and n (to be clarified later); in terms of applications, the availability of the fast-rate model with period h broadens the choices for multirate control design; the relaxation of assumptions makes identification of fast-rate models for more general MRSD systems possible, e.g., the input updating rates for MIMO MRSD systems no longer have to be uniform or be faster than the output sampling rates.

The question states precisely as follows: For a sampling period h, the unknown continuous-time system G_c has a discrete-time counterpart realized by the step-invariant-transformation, $G_d := S_h G_c H_h$, represented by a state-space model:

$$D + C\,(zI - A)^{-1}\,B =: \left[\begin{array}{c|c} A & B \\ \hline C & D \end{array}\right]. \tag{1.1}$$

Given the multirate input-output data in Figure 1.1, how to identify the so-called fast-rate system G_d?

As an important part in system identification field, closed-loop systems have long been of prime interest both in academic research and in industrial application. One of the kernel topics is identifiability. For a closed-loop system with linear output feedback, it is well-known that identifiability is ensured by adding an external persistently exciting test signal [17]. However, adding such a signal sometimes is undesirable, since it usually disturbs the normal operation or affects product qualities. Is it possible to achieve identifiability without external excitations?[3]

To answer the first question, we start in Chapter 2 with using the lifting technique to associate such an LPTV system with an LTI system, the so-called lifted system. Chapter 3 studies the uniqueness of recovering the fast-rate system from the lifted system, and analyzes controllability and observability of the lifted system, which are essential to the identifiability issue. Chapter 4 presents time-domain and frequency-domain approaches to compute a fast-

[2]Henceforth, a system or a model with period h means that its sampling period is h.
[3]A more detailed introduction is in Chapter 6.

rate model and illustrates the effectiveness of the proposed methods through examples. All previous chapters have focused on SISO systems for the sake of an easier presentation. In Chapter 5, after an investigation of the noise system estimation we give a discussion about the extension into MIMO systems. Chapter 6 deals with the second question, identification of closed-loop systems without external excitation, where the fast-sampling direct approach is proposed with an identifiability analysis. Finally, Chapter 7 summarizes the thesis by listing its main contributions and unsolved problems.

Chapter 2

Lifting Signals and Systems

In this chapter, we will associate a SISO MRSD system that is essentially LPTV with a lifted LTI system using the lifting technique.

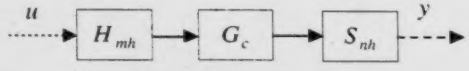

Figure 2.1: A SISO noise-free MRSD system

Let us start with a question: why is it LPTV? The MRSD system in Figure 2.1, which is a noise-free version of Figure 1.1, has an input-output property that shifting the input u by n samples results in shifting the output y by m samples. Such a property is called as (m,n)-shift invariance, represented by

$$(S_{nh}G_cH_{mh})U^n = U^m(S_{nh}G_cH_{mh}). \tag{2.1}$$

Here U is the discrete-time unit time-delay operator and its left inverse U^* is the discrete-time unit time-advance operator. Note that $U^*U = I$, $UU^* \neq I$. To see (2.1), we need some identities

$$S_{nh} = S_nS_h,\ H_{mh} = H_hH_m,\ H_mU^n = U^{mn}H_m,\ S_nU^{mn} = U^mS_n. \tag{2.2}$$

Here S_n is the discrete-time down-sampler by a factor of n, defined as taking an input sequence $x(k)$ and produces the output sequence

$$y(k) = x(kn). \tag{2.3}$$

H_m is the discrete-time zero-order-hold by a factor of m, defined as taking an input sequence $x(k)$ and produces an output sequence

$$y\,(k) = x\left(\left\lfloor \frac{k}{m} \right\rfloor_{\text{Int}}\right), \tag{2.4}$$

where $\lfloor \frac{k}{m} \rfloor_{\text{Int}}$ means the floor function, giving the largest integer less than or equal to k/m. Based on these, we have

$$\begin{aligned} S_{nh}G_cH_{mh}U^n &= S_nS_hG_cH_hH_mU^n \\ &= S_nG_dU^{mn}H_m \\ &= S_nU^{mn}G_dH_m \\ &= U^mS_nG_dH_m \\ &= U^mS_{nh}G_cH_{mh} \end{aligned}$$

by time-invariance of $G_d := S_hG_cH_h$ and the properties in (2.2). In real time, the MRSD system $S_{nh}G_cH_{mh}$ is periodic with period mnh, in the sense that shifting the input by mnh timescales corresponds to shifting the output by the same amount of timescales.[1]

Now we introduce the lifting technique. Let l be the space of discrete-time signals – real and perhaps vector valued – defined on the time set $\{0, 1, 2, \cdots\}$, i.e., the nonnegative integer set $\mathbb{Z}_+$. A signal ψ in l can be written

$$\psi = \{\psi(0), \psi(1), \psi(2), \cdots\}.$$

For a positive integer n, the n-fold discrete lifting operator L_n is defined as the mapping from ψ to $\underline{\psi}$, where underlining denotes lifting:

$$\{\psi(0), \psi(1), \cdots\} \mapsto \left\{ \begin{bmatrix} \psi(0) \\ \psi(1) \\ \vdots \\ \psi(n-1) \end{bmatrix}, \begin{bmatrix} \psi(n) \\ \psi(n+1) \\ \vdots \\ \psi(2n-1) \end{bmatrix}, \cdots \right\}. \tag{2.5}$$

Thus, L_n maps l to l^n, the external direct sum of n copies of l. If the underlying period of ψ is h, that of the lifted signal $\underline{\psi}$ is nh. The inverse of the lifting operator, L_n^{-1}, is defined as the inverse operation of (2.5), i.e., $L_n^{-1}L_n = I$ and $L_nL_n^{-1} = I$.

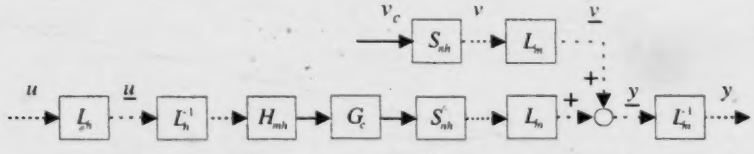

Figure 2.2: The lifted multirate sampled-data system

In Figure 2.2, we lift u by L_n into $\underline{u}$, and lift y by L_m into $\underline{y}$. The disturbance v_c is fictitiously sampled into v with period nh, same as the output sampling period, and v is

[1]Strictly speaking, MRSD systems are better called (m, n)-shift invariant systems instead of periodic systems to avoid confusion.

lifted by L_m into $\underline{v}$. Thus, $\underline{u}$, $\underline{y}$ and $\underline{v}$ share the same period mnh, and form a discrete-time LTI system [13]:

$$\underline{y} = \underline{G_d}\,\underline{u} + \underline{v}. \tag{2.6}$$

Here $\underline{G_d}$ is the so-called lifted system from $\underline{u}$ to $\underline{y}$, i.e., $\underline{G_d} = L_m S_{nh} G_c H_{mh} L_n^{-1}$. To show that G_d is LTI, it suffices to show $U^* \underline{G_d} U = \underline{G_d}$. By identities $L_n^{-1} U = U^n L_n^{-1}$, $U^* L_n = L_n (U^*)^n$, and (m,n)-shift invariance of $S_{nh} G_c H_{mh}$, we get

$$\begin{aligned} U^* \underline{G_d} U &= U^* L_m S_{nh} G_c H_{mh} L_n^{-1} U \\ &= L_m (U^*)^m S_{nh} G_c H_{mh} U^n L_n^{-1} \\ &= L_m S_{nh} G_c H_{mh} L_n^{-1} \\ &= \underline{G_d}. \end{aligned}$$

$\underline{G_d}$ has a state-space representation by matrices $\underline{A}$, $\underline{B}$, $\underline{C}$ and $\underline{D}$, which are related to A, B, C and D of (1.1) as shown in Chen and Qiu [4]:

$$\left[\begin{array}{c|c} \underline{A} & \underline{B} \\ \hline \underline{C} & \underline{D} \end{array}\right] := \left[\begin{array}{c|ccc} A^{mn} & \sum_{i=mn-m}^{mn-1} A^i B & \sum_{i=mn-2m}^{mn-m-1} A^i B & \cdots & \sum_{i=0}^{m-1} A^i B \\ \hline C & D_{00} & D_{01} & \cdots & D_{0,n-1} \\ CA^n & D_{10} & D_{11} & \cdots & D_{1,n-1} \\ \vdots & \vdots & \vdots & & \vdots \\ CA^{mn-n} & D_{m-1,0} & D_{m-1,1} & \cdots & D_{m-1,n-1} \end{array}\right], \tag{2.7}$$

where

$$D_{ij} = D\chi_{[jm,(j+1)m)}(in) + \sum_{r=jm}^{(j+1)m-1} CA^{in-1-r} B \chi_{[0,in)}(r)$$

and a characteristic function on integers is defined:

$$\chi_{[a,b)}(r) = \begin{cases} 1, & a \le r < b \\ 0, & \text{otherwise.} \end{cases}$$

Here we use examples to illustrate (2.7).

Example 2.1

If $m = 2$, $n = 3$, i.e., $\underline{G_d} = L_2 S_{3h} G_c H_{2h} L_3^{-1}$, we have

$$\begin{aligned} \underline{G_d} &= L_2 S_{3h} G_c H_{2h} L_3^{-1} \\ &= L_2 S_{3h} H_h S_h G_c H_h S_h H_{2h} L_3^{-1} \\ &= \left(L_2 S_{3h} H_h L_6^{-1}\right)\left(L_6 G_d L_6^{-1}\right)\left(L_6 S_h H_{2h} L_3^{-1}\right). \end{aligned} \tag{2.8}$$

by properties $S_{3h} = S_{3h}H_hS_h$, $H_{2h} = H_hS_hH_{2h}$, $L_6^{-1}L_6 = I$ and $L_6L_6^{-1} = I$ [5]. The transfer matrix of $L_6G_dL_6^{-1}$ is [21]

$$\left[\begin{array}{c|cccccc} A^6 & A^5B & A^4B & A^3B & A^2B & AB & B \\ \hline C & D & 0 & 0 & 0 & 0 & 0 \\ CA & CB & D & 0 & 0 & 0 & 0 \\ CA^2 & CAB & CB & D & 0 & 0 & 0 \\ CA^3 & CA^2B & CAB & CB & D & 0 & 0 \\ CA^4 & CA^3B & CA^2B & CAB & CB & D & 0 \\ CA^5 & CA^4B & CA^3B & CA^2B & CAB & CB & D \end{array}\right]. \tag{2.9}$$

The transfer matrix of $L_2S_{3h}H_hL_6^{-1}$ is [5]

$$\left[\begin{array}{cccccc} I & 0 & 0 & 0 & 0 & 0 \\ 0 & 0 & 0 & I & 0 & 0 \end{array}\right], \tag{2.10}$$

and that of $L_6S_hH_{2h}L_3^{-1}$ is

$$\left[\begin{array}{cccccc} I & I & 0 & 0 & 0 & 0 \\ 0 & 0 & I & I & 0 & 0 \\ 0 & 0 & 0 & 0 & I & I \end{array}\right]^T. \tag{2.11}$$

From (2.9), (2.10) and (2.11), the transfer matrix of $\underline{G_d}$ is

$$\begin{aligned} \left[\begin{array}{c|c} \underline{A} & \underline{B} \\ \hline \underline{C} & \underline{D} \end{array}\right] &:= \left[\begin{array}{cccccc} I & 0 & 0 & 0 & 0 & 0 \\ 0 & 0 & 0 & I & 0 & 0 \end{array}\right] \cdot \left\{ \left[\begin{array}{cccccc} D & 0 & 0 & 0 & 0 & 0 \\ CB & D & 0 & 0 & 0 & 0 \\ CAB & CB & D & 0 & 0 & 0 \\ CA^2B & CAB & CB & D & 0 & 0 \\ CA^3B & CA^2B & CAB & CB & D & 0 \\ CA^4B & CA^3B & CA^2B & CAB & CB & D \end{array}\right] + \right. \\ &\left. \left[\begin{array}{c} C \\ CA \\ CA^2 \\ CA^3 \\ CA^4 \\ CA^5 \end{array}\right] \left(zI - A^6\right) \left[\begin{array}{cccccc} A^5B & A^4B & A^3B & A^2B & AB & B \end{array}\right] \right\} \cdot \left[\begin{array}{ccc} I & 0 & 0 \\ I & 0 & 0 \\ 0 & I & 0 \\ 0 & I & 0 \\ 0 & 0 & I \\ 0 & 0 & I \end{array}\right] \\ &= \left[\begin{array}{c|ccc} A^6 & \left(A^5 + A^4\right)B & \left(A^3 + A^2\right)B & (A + I)B \\ \hline C & D & 0 & 0 \\ CA^3 & C\left(A^2 + A\right)B & CB + D & 0 \end{array}\right]. \end{aligned} \tag{2.12}$$

Example 2.2

If $m = 3$, $n = 2$, i.e., the dual of Example 2.1, (2.7) becomes

$$\left[\begin{array}{c|c} \underline{A} & \underline{B} \\ \hline \underline{C} & \underline{D} \end{array}\right] := \left[\begin{array}{c|cc} A^6 & A^5B + A^4B + A^3B & A^2B + AB + B \\ \hline C & D & 0 \\ CA^2 & CAB + CB + D & 0 \\ CA^4 & CA^3B + CA^2B + CAB & CB + D \end{array}\right]. \tag{2.13}$$

Note that lifting also has some disadvantages. One of them is the so-called causality constraint, i.e., $\underline{D}$ in (2.7) is (block) lower triangular, e.g., those in (2.12) and (2.13). Another is the increase of dimensions, e.g., SISO systems become MIMO or some of the system matrices grow larger.

A noise model can be used to further describe the characteristics of the noise term $\underline{v}$ in (2.6). To ease the problem, we adopt an output error model structure, since output error models will give consistent estimates for open-loop systems, even if the additive noise is not white [29]. An innovation form of the state-space model with the Kalman filter gain $\underline{K} = 0$ represents the overall lifted system:

$$\dot{x} = \underline{A}\,x + \underline{B}\,\underline{u} + \underline{K}\,\underline{e}, \tag{2.14a}$$

$$\underline{y} = \underline{C}\,x + \underline{D}\,\underline{u} + \underline{e}. \tag{2.14b}$$

Here overdot denotes forward time advance, for example, $\dot{\psi}(k) := \psi(k+1)$. $\underline{e}$ is a white noise vector, and x is a state vector. If p is the order of G_d, then the dimensions of A, B, C, D are $p \times p$, $p \times 1$, $1 \times p$, and 1×1, respectively, and those of $\underline{A}$, $\underline{B}$, $\underline{C}$, $\underline{D}$, $\underline{K}$ are $p \times p$, $p \times n$, $m \times p$, $m \times n$, and $p \times m$, respectively. Note that $\underline{A}$, $\underline{B}$, $\underline{C}$ and $\underline{D}$ will be same as those in (2.7) only if an output error model structure is adopted. Otherwise, a noise model may introduce extra states such that $\underline{A}$ and A may not share the same dimension.[2]

[2]It is further discussed in Chapter 5.

Chapter 3

Identifiability Analysis

In Chapter 2, we associate an LPTV system with an LTI one using the lifting technique, which brings the original problem into the traditional system identification framework – a well-established field. However, MRSD systems give rise to new challenges. Some of them are closely related to the identifiability issue, namely, uniqueness of the fast-rate system, controllability and observability of the lifted system, and so on, which are the topics of the current chapter.

3.1 Uniqueness of Fast-Rate Systems

Before starting the exploration of recovering the fast-rate system G_d from the lifted system $\underline{G_d}$, a question arises naturally: Is the recovery unique? The answer is affirmative if and only if m and n are coprime. We observe from Figure 2.2:

$$\begin{aligned} \underline{G_d} &= L_m S_{nh} G_c H_{mh} L_n^{-1} \\ &= L_m S_n \left(S_h G_c H_h\right) H_m L_n^{-1} \\ &= L_m S_n G_d H_m L_n^{-1}, \end{aligned} \tag{3.1}$$

by properties $S_{nh} = S_n S_h$ and $H_{mh} = H_h H_m$. Since the lifting operation is one-to-one, the problem of recovery of a unique G_d from $\underline{G_d}$ is equivalent to answering a question: Is the mapping $G_d \longmapsto S_n G_d H_m$ one-to-one?[1]

Proposition 1 *Assume G_d is LTI and causal. Then, the mapping $G_d \longmapsto S_n G_d H_m$ is one-to-one if and only if m and n are coprime.*

Proof: For sufficiency[2], it suffices to show that $S_n G_d H_m = 0$ implies $G_d = 0$ if m and n are coprime. Let us assume $S_n G_d H_m = 0$ and let μ be the impulse response of G_d, i.e.,

[1] One-to-one means bijective.

[2] This part is similar to the proof of *Lemma* 5 in [6].

$\mu = G_d\delta$, where δ is the discrete-time unit impulse signal. It follows that for any integer i, $S_nG_dH_mU^i\delta = 0$, where U is the unit time-delay operator. This implies, by the definition (2.4) of H_m,

$$S_nG_d\left(U^{im} + U^{im+1} + \cdots + U^{im+m-1}\right)\delta = 0.$$

The time invariance of G_d and the definition (2.3) of S_n imply

$$\mu(im+jn) + \mu(im+jn+1) + \cdots + \mu(im+jn+m-1) = 0,\ \forall i,\ j. \tag{3.2}$$

Since m and n are coprime, there exist integers m' and n' such that $mm' + nn' = 1$. Thus, for any k, there always exist $i = km'$ and $j = kn'$ in (3.2) to get $im + jn = k$. Hence,

$$\mu(k) + \mu(k+1) + \cdots + \mu(k+m-1) = 0, \forall k. \tag{3.3}$$

By causality of $\mu(k)$, (3.3) implies that $\mu(k) = 0$, $\forall k$, e.g., if $k = -(m-1)$, then $\mu(0) = 0$; if $k = -(m-2)$, then $\mu(1) = 0$ and so on. Hence, $G_d = 0$.

The necessity is proved as follows. If m and n are not coprime, there exists a common factor k: $m = km', n = kn'$, where m' and n' are coprime. It follows from (3.1) that $S_nG_dH_m = S_{n'}G_{kd}H_{m'}$, where $G_{kd} = S_{kh}G_cH_{kh}$, i.e., a discrete-time counterpart of G_c with period kh. Thus, the mapping $G_d \longmapsto S_nG_dH_m$ is not one-to-one, since the mapping $G_d \longmapsto G_{kd} = S_kG_dH_k$ is known to be not injective. □

In the sequel, we assume that m and n are coprime in order to get a unique fast-rate system. Note that any common factor of m and n can be absorbed into h.

3.2 Controllability and Observability of Lifted Systems

For a state-space system to be identifiable, e.g., minimal realizations, the lifted system $\underline{G_d}$ in general needs to be controllable and observable. If the continuous-time system G_c is controllable and observable and the sampling period is non-pathological, then the discrete-time system G_d is also controllable and observable [20], which is still valid if a continuous time delay exists. Francis and Georgiou [13] have proved that if G_d is stabilizable and detectable, and satisfies an additional condition (*): For every eigenvalue λ of A, none of the $mn-1$ points

$$\lambda e^{j\frac{2\pi k}{mn}}, k = 1, 2, \cdots, mn-1$$

is an eigenvalue of A, then $\left(A^{mn}, A^iB\right)$ is stabilizable and $\left(CA^i, A^{mn}\right)$ is detectable for any positive integer i. Based on the above statements, we reach:

Proposition 2 *Assume A satisfies the condition $(*)$. If (C, A) is observable, so is $(\underline{C}, \underline{A})$; if (A, B) is controllable and A has no eigenvalues on the unit circle, $(\underline{A}, \underline{B})$ is also controllable.*

Proof: The first part follows with some trivial modifications from Lemma 6 in Francis and Georgiou [13] in which $\left(CA^i, \underline{A}\right)$ was shown detectable. We prove the second part by showing that $\left(\underline{A}, \sum_{i=0}^{m-1} A^i B\right)$ is controllable, i.e., all eigenvalues of $\underline{A}$ are controllable. Now each eigenvalue of $\underline{A}$ has the form λ^{mn}, where λ is an eigenvalue of A. Define functions:

$$g(s) := \frac{s^{mn} - \lambda^{mn}}{s - \lambda}, \; f(s) := \sum_{i=0}^{m-1} s^i.$$

By non-pathological sampling, $g(A)$ is invertible (see Theorem 3.2.1 in [5]). If A has no eigenvalues on the unit circle, then $\sum_{i=0}^{m-1} \lambda^i \neq 0$. Thus $f(A)$ is invertible. Therefore,

$$\begin{aligned}
& \operatorname{rank}\left(\left[\begin{array}{cc} (A^{mn} - \lambda^{mn} I) & \sum_{i=0}^{m-1} A^i B \end{array}\right]\right) \\
= \; & \operatorname{rank}\left(\left[\begin{array}{cc} (A - \lambda I)\, g(A) & f(A)\, B \end{array}\right]\right) \\
= \; & \operatorname{rank}\left(f(A) \left[\begin{array}{cc} A - \lambda I & B \end{array}\right] \left[\begin{array}{cc} f^{-1}(A)\, g(A) & 0 \\ 0 & I \end{array}\right]\right) \\
= \; & \operatorname{rank}\left(\left[\begin{array}{cc} A - \lambda I & B \end{array}\right]\right),
\end{aligned}$$

where the second equality holds because $f(A)$ is a polynomial of A so that the commutativity holds. Thus, $(\underline{A}, \underline{B})$ is controllable. □

Note that the conditions in Proposition 2 are not necessary conditions. Violations of them will not necessarily lead to the loss of controllability or/and observability. However, if there exists a continuous time delay τ larger than h, A will have at least two poles at the origin [2], i.e., the condition $(*)$ will be violated. Observability has been shown to be lost and a remedy is proposed by Li *et al.* [27], which is summarized below: First, we can identify an $m \times n$ time-delay matrix Γ from $\underline{u}$, $\underline{y}$ using a correlation analysis [22]:

$$\Gamma = \left[\begin{array}{cccc} l_{00} & l_{01} & \cdots & l_{0,n-1} \\ l_{10} & l_{11} & \cdots & l_{1,n-1} \\ \vdots & \vdots & & \vdots \\ l_{m-1,0} & l_{m-1,1} & \cdots & l_{m-1,n-1} \end{array}\right],$$

where l_{ij} is the estimated time delay (a nonnegative integer) from the j-th input $\underline{u}_j$ to the i-th output $\underline{y}_i$, $i = 0, 1, \cdots, m-1$ and $j = 0, 1, \cdots, n-1$. The relation between l_{ij} and τ is given by (see (A-3)):

$$(l_{ij} - 1)\, mnh < \tau + jmh - inh \leq l_{ij} mnh. \tag{3.4}$$

Second, there exists a one-to-one correspondence between Γ and a positive integer k such that τ is estimated as (see Appendix A for a proof):

$$kh < \hat{\tau} \leq kh + h. \tag{3.5}$$

Third, since m and n are coprime, there exist integers k_1 and k_2 such that

$$k = k_1 m + k_2 n. \tag{3.6}$$

Finally, we shift the measured input data, $u_s[l] = u[l - k_1]$, and shift the measured output data, $y_s[l] = y[l + k_2]$, so that, the time delay between u_s and y_s is not larger than h. Hence, controllability and observability will be preserved.

Example 3.1

We illustrate the idea by estimating the time delay of Example 4.1, where $m = 3$, $n = 2$ and $h = 1$ sec. Γ is estimated as:

$$\hat{\Gamma} = \begin{bmatrix} 2 & 2 \\ 1 & 2 \\ 1 & 1 \end{bmatrix}.$$

From (3.4), we have

$$\begin{aligned} 6 < \hat{\tau} \leq 12 \quad &, \quad 3 < \hat{\tau} \leq 9, \\ 2 < \hat{\tau} \leq 8 \quad &, \quad 5 < \hat{\tau} \leq 11, \\ 4 < \hat{\tau} \leq 10 \quad &, \quad 1 < \hat{\tau} \leq 7. \end{aligned}$$

These inequalities give $6 < \hat{\tau} \leq 7$, i.e., $k = 6$ in (3.5). Next, we shift the measured input and output data according to (3.6): $6 = 3k_1 + 2k_2$, say, $k_1 = 0$ and $k_2 = 3$, i.e., keep u unchanged as u_s and shift y by time advancing by 3 samples: $y_s[l] = y[l + 3]$. Effectiveness is confirmed by estimating the time delay between u_s and y_s in the same way.

Chapter 4

Fast-Rate Model Computation

In Chapter 2, we associate the original LPTV MRSD system with an equivalent LTI system, i.e., the so-called lifted system $\underline{G_d}$, using the lifting technique. Afterwards, we discuss some identifiability concerns. In the sequel, we therefore assume that an estimate of the lifted system, $\underline{\hat{G}_d}$, will converge to the true system $\underline{G_d}$ under the mild conditions[1] introduced in Chapter 3. In this chapter, two approaches in the time domain and one in the frequency domain are proposed to compute the fast-rate system G_d after $\underline{G_d}$ has been estimated. Their effectiveness is demonstrated through simulation and real-time implementation.

4.1 Time-Domain Approach

Once $\underline{G_d}$ is estimated, i.e., $\underline{A}$, $\underline{B}$, $\underline{C}$ and $\underline{D}$ in (2.7) are known, how to extract matrices A, B and C? Note $D = 0$ for a strictly causal system. The difficulty lies in that in general A cannot be determined by taking the mn-th roots of $\underline{A}$. Once $\hat{A}$, an estimate of A, is known, and $\underline{B}$, $\underline{C}$ in (2.7) are partitioned as

$$\underline{\hat{B}} = \begin{bmatrix} B_1 & B_2 & \cdots & B_n \end{bmatrix}, \tag{4.1}$$

$$\underline{\hat{C}} = \begin{bmatrix} C_1^T & C_2^T & \cdots & C_m^T \end{bmatrix}^T, \tag{4.2}$$

where $B_1, B_2, \cdots, B_n \in \mathbb{R}^{p\times 1}$, and $C_1, C_2, \cdots, C_m \in \mathbb{R}^{1\times p}$ (p is the order of G_d), then, B and C can be determined as

$$\hat{C} = C_1, \ \hat{B} = \left(\sum_{i=0}^{m-1} \hat{A}^i\right)^{-1} B_n. \tag{4.3}$$

The proof of Proposition 2 shows the existence of the inverse in (4.3) if the conditions in Proposition 2 are true.

[1] Formally, we also need other conditions like those standard in the traditional identification.

Another way of computing B and C is to include other partitioned matrices in (4.1) and (4.2), and use the least-squares method. For instance,

$$\hat{C} = \Phi\Phi_c^T \left(\Phi_c\Phi_c^T\right)^{-1},$$

where

$$\Phi = \left[\begin{array}{cccc} C_1 & C_2 & \cdots & C_m \end{array}\right],$$

$$\Phi_c = \left[\begin{array}{cccc} I & \hat{A}^n & \cdots & \hat{A}^{mn-n} \end{array}\right].$$

A. Controllability and Observability Approach

We propose two time-domain approaches to compute the matrix A. The first one, the controllability and observability approach, is based on assumptions that (A_{mh}, B_{mh}) is controllable and (C, A_{nh}) is observable, where

$$A_{mh} := A^m,\ A_{nh} := A^n,$$

$$B_{mh} := B_n = \sum_{i=0}^{m-1} A^i B.$$

Similar to the proof of Proposition 2, both assumptions can be shown to be valid if the conditions in Proposition 2 are true. This approach consists of three steps:
Step 1: Given $\underline{A}$ and $\underline{B}$ partitioned in (4.1), (2.7) implies

$$A_{mh}^n = \underline{A},$$

$$B_{mh} = B_n,\ A_{mh}B_{mh} = B_{n-1},\ \cdots,\ A_{mh}^{n-1}B = B_1.$$

Thus, $A_{mh}^k B_{mh}$ is known for any $k \geq 0$. We form the controllability matrix Ω_c of (A_{mh}, B_{mh}) and the shifted controllability matrix Ω:

$$\Omega_c = \left[\begin{array}{cccc} B_{mh} & A_{mh}B_{mh} & \cdots & A_{mh}^{p-1}B_{mh} \end{array}\right],$$

$$\Omega = \left[\begin{array}{cccc} A_{mh}B_{mh} & A_{mh}^2B_{mh} & \cdots & A_{mh}^{p}B_{mh} \end{array}\right].$$

Since $A_{mh}\Omega_c = \Omega$ and the controllability assumption implies that Ω_c is full row rank, A_{mh} is uniquely determined by

$$\hat{A}_{mh} = \Omega\Omega_c^T \left(\Omega_c\Omega_c^T\right)^{-1}.$$

Step 2: Given $\underline{A}$ and $\underline{C}$ partitioned in (4.2), (2.7) implies

$$A_{nh}^m = \underline{A},$$

$$C = C_1,\ CA_{nh} = C_2,\ \cdots,\ CA_{nh}^{m-1} = C_m.$$

Thus, CA_{nh}^k is known for any $k \geq 0$. We form the observability matrix Ψ_o of (C, A_{nh}) and the shifted observability matrix Ψ:

$$\Psi_o = \begin{bmatrix} C \\ CA_{nh} \\ \vdots \\ CA_{nh}^{p-1} \end{bmatrix},\ \Psi = \begin{bmatrix} CA_{nh} \\ CA_{nh}^2 \\ \vdots \\ CA_{nh}^{p} \end{bmatrix}.$$

Since $\Psi_o A_{nh} = \Psi$ and the observability assumption implies that Ψ_o is full column rank, A_{nh} is uniquely determined by

$$\hat{A}_{nh} = \left(\Psi_o^T \Psi_o\right)^{-1} \Psi_o^T \Psi.$$

Step 3: Now, $A_{mh} = A^m$ and $A_{nh} = A^n$ are estimated. Since m and n are coprime, there always exist two integers m', n' such that

$$nn' - mm' = 1.$$

Thus, we have:

$$\left(A_{mh}\right)^{m'} A = \left(A_{nh}\right)^{n'}.$$

If A is invertible,

$$\hat{A} = \left(\hat{A}_{mh}^{m'}\right)^{-1} \left(\hat{A}_{nh}\right)^{n'};$$

otherwise,

$$\hat{A} = \left(\hat{A}_{mh}^{m'}\right)^{\dagger} \left(\hat{A}_{nh}\right)^{n'},$$

where $\dagger$ denotes a pseudo-inverse.

Remark 1: In practice, time delays usually exist, i.e., A has at least a pole at the origin. Since applying the remedy in Chapter 3 will only guarantee that at most one pole is at the origin for the system estimated from the shifted data, $\hat{A}_{mh}$ or $\hat{A}_{nh}$ is often singular or nearly singular indicated by a large condition number. The inverse will be replaced by a pseudo-inverse. Most often, a good estimate of A is achieved by using the reduced singular value decomposition to realize the pseudo-inverse [24].

Remark 2: This approach relies heavily on the structures of matrices shown in (2.7). To achieve such structures, a state-space model with coupled parameters [30], the so-called "greybox" model can be used. Numerically, it is indeed a constrained nonlinear optimization problem.

B. Matrix Roots Approach

The second approach, the matrix roots approach, is based on a condition that $\underline{A}$ is diagonalizable, i.e.,

$$P^{-1}\underline{A}P = \text{diag}\,(\lambda_1, \lambda_2, \cdots, \lambda_p)\,,$$

where λ_1, λ_2, $\cdots$, λ_p are eigenvalues of $\underline{A}$ and P is the corresponding eigenvector matrix. Since $\underline{A} = A^{mn}$, A and $\underline{A}$ share same eigenvectors. If $\rho_i = \alpha_i + j\beta_i$ is a pole of G_c, then

$$\lambda_i = e^{mnh\rho_i} = e^{mnh\alpha_i} e^{jmnh\beta_i}.$$

With an assumption $|mnh\beta_i| < \pi$ for $i = 1, \cdots, p$,

$$A = P\,\text{diag}\left(\lambda_1^{\frac{1}{mn}}, \lambda_2^{\frac{1}{mn}}, \cdots, \lambda_p^{\frac{1}{mn}}\right) P^{-1},$$

where $\lambda_i^{\frac{1}{mn}}$ is the n-th principal root of λ_i.

Remark: In practice, the assumption that $|mnh\beta_i| < \pi$ for $i = 1, \cdots, p$ is unable to be checked. If this assumption is not true, indicated by an unsatisfactory $\hat{G}_d$, A may be found by searching through all mn-th roots of $\underline{A}$.

4.2 Frequency-Domain Approach

As a powerful tool, the polyphase decomposition can be used to compute the transfer function of G_d after $\underline{G_d}$ has been estimated. For ease of discussion, let us illustrate the idea through Example 4.1, where $m = 3$, $n = 2$ and $h = 1$ sec. With identities [5]

$$H_{3h} = H_h S_h H_{3h},\ S_{2h} = S_{2h} H_h S_h,\ L_6^{-1} L_6 = I,\ L_6 L_6^{-1} = I,$$

$\underline{G_d}$ in (3.1) can be written as

$$\begin{aligned} \underline{G_d} &= L_3 S_{2h} G_c H_{3h} L_2^{-1} \\ &= L_3 S_{2h} H_h S_h G_c H_h S_h H_{3h} L_2^{-1} \\ &= \underbrace{\left(L_3 S_{2h} H_h L_6^{-1}\right)}_{S_L} \underbrace{\left(L_6 G_d L_6^{-1}\right)}_{G_L} \underbrace{\left(L_6 S_h H_{3h} L_2^{-1}\right)}_{H_L}. \end{aligned} \tag{4.4}$$

S_L and H_L in (4.4) are constant matrices [5]:

$$S_L = \begin{bmatrix} I & 0 & 0 & 0 & 0 & 0 \\ 0 & 0 & I & 0 & 0 & 0 \\ 0 & 0 & 0 & 0 & I & 0 \end{bmatrix},\ H_L = \begin{bmatrix} I & 0 \\ I & 0 \\ I & 0 \\ 0 & I \\ 0 & I \\ 0 & I \end{bmatrix}. \tag{4.5}$$

The transfer matrix of G_L in (4.4), represented in the polyphase decomposition form, is a Toeplitz matrix (also called as a pseudo-circulant matrix [36]) given by Khargonekar *et al.* [21]:

$$\hat{g}_L = \begin{bmatrix} g_0(z) & z^{-1}g_5(z) & z^{-1}g_4(z) & z^{-1}g_3(z) & z^{-1}g_2(z) & z^{-1}g_1(z) \\ g_1(z) & g_0(z) & z^{-1}g_5(z) & z^{-1}g_4(z) & z^{-1}g_3(z) & z^{-1}g_2(z) \\ g_2(z) & g_1(z) & g_0(z) & z^{-1}g_5(z) & z^{-1}g_4(z) & z^{-1}g_3(z) \\ g_3(z) & g_2(z) & g_1(z) & g_0(z) & z^{-1}g_5(z) & z^{-1}g_4(z) \\ g_4(z) & g_3(z) & g_2(z) & g_1(z) & g_0(z) & z^{-1}g_5(z) \\ g_5(z) & g_4(z) & g_3(z) & g_2(z) & g_1(z) & g_0(z) \end{bmatrix}. \tag{4.6}$$

Here $g_0(z)$, $g_1(z)$, $\cdots$, $g_5(z)$ are defined in the polyphase decomposition of G_d introduced by Davis [10]:

$$\begin{aligned} \hat{g}_d(z) &= g(0) + z^{-1}g(1) + z^{-2}g(2) + \cdots \\ &= \left[g(0) + z^{-6}g(6) + \cdots\right] + z^{-1}\left[g(1) + z^{-6}g(7) + \cdots\right] \\ &\quad + \cdots + z^{-5}\left[g(5) + z^{-6}g(11) + \cdots\right] \\ &= : g_0\left(z^6\right) + z^{-1}g_1\left(z^6\right) + \cdots + z^{-5}g_5\left(z^6\right). \end{aligned} \tag{4.7}$$

From (4.4), (4.5) and (4.6), the transfer matrix of $\underline{G_d}$ in the polyphase decomposition form is obtained by retaining the first, the third and the fifth rows and adding every three columns starting from the upper-left corner of (4.6):

$$\begin{aligned} \underline{\hat{g}_d} &= \begin{bmatrix} G_{11} & G_{12} \\ G_{21} & G_{22} \\ G_{31} & G_{32} \end{bmatrix} \\ &= \begin{bmatrix} g_0(z) + z^{-1}g_5(z) + z^{-1}g_4(z) & z^{-1}g_3(z) + z^{-1}g_2(z) + z^{-1}g_1(z) \\ g_2(z) + g_1(z) + g_0(z) & z^{-1}g_5(z) + z^{-1}g_4(z) + z^{-1}g_3(z) \\ g_4(z) + g_3(z) + g_2(z) & g_1(z) + g_0(z) + z^{-1}g_5(z) \end{bmatrix}. \end{aligned} \tag{4.8}$$

Thus, we can establish six linear equations from (4.8), written in a matrix form:

$$\begin{bmatrix} I & 0 & 0 & 0 & z^{-1} & z^{-1} \\ 0 & z^{-1} & z^{-1} & z^{-1} & 0 & 0 \\ I & I & I & 0 & 0 & 0 \\ 0 & 0 & 0 & z^{-1} & z^{-1} & z^{-1} \\ 0 & 0 & I & I & I & 0 \\ I & I & 0 & 0 & 0 & z^{-1} \end{bmatrix} \begin{bmatrix} g_0(z) \\ g_1(z) \\ g_2(z) \\ g_3(z) \\ g_4(z) \\ g_5(z) \end{bmatrix} = \begin{bmatrix} G_{11} \\ G_{12} \\ G_{21} \\ G_{22} \\ G_{31} \\ G_{32} \end{bmatrix}. \tag{4.9}$$

If $\underline{G_d}$ is estimated from the input-output data, i.e., G_{11}, G_{12}, $\cdots$, G_{32} are known, then $g_0(z)$, $g_1(z)$, $\cdots$, $g_5(z)$ are uniquely determined, since the square matrix in (4.9) is nonsingular. Therefore, the transfer matrix of G_d is determined uniquely by (4.7):

$$\hat{g}_d(z) = \hat{g}_0\left(z^6\right) + z^{-1}\hat{g}_1\left(z^6\right) + \cdots + z^{-5}\hat{g}_5\left(z^6\right). \tag{4.10}$$

The procedure for this specific example can be generalized in a straightforward manner. However, this approach usually gives a high order model. We can realize this point through (4.10), where z^6 is the operator. Thus, the approach requires more effort, e.g., model reduction may be required. Even so, it is still an insightful approach especially for theoretical analysis. For instance, feasibility and uniqueness of getting a fast-rate model are illustrated very clearly in this example. As an contrary example, if m and n are not coprime, say $m = 4$ and $n = 2$, then the corresponding square matrix in (4.9) will be singular, i.e., uniqueness is lost.

4.3 Examples

Before giving examples, we are in a position to discuss some practical issues about implementation of the proposed approaches and summarize an identification procedure.

Causality constraints: Lifting causes a causality constraint, i.e., $\underline{D}$ in (2.7) is (block) lower triangular. How to identify a model with such a constraint? A modified sub-space identification algorithm was proposed by Li *et al.* [27]. As an easier alternative, a structured state-space model with free parameters [30] can be used to deal with the constraint, which makes existing standard identification algorithms applicable. For instance, $\underline{D}$ in (2.13), where $m = 3$ and $n = 2$, can be parameterized as

$$\begin{bmatrix} 0 & 0 \\ \times & 0 \\ \times & \times \end{bmatrix},$$

where $\times$ marks an adjustable parameter. Note that G_c is strictly causal in practice such that $D = 0$.

Model validation: It is straightforward to validate the estimated fast-rate model in simulation or in experiments, since the true system or/and the fast-rate input and output data are accessible. However, in practice, all of them are unknown, which means that the fast-rate model validation cannot be implemented directly. An intuitive way is to put the estimated fast-rate model into the same framework as the original system and compare the estimated output with the measured output through some criteria, such as the one based on the mean square errors. Note that the work by Chai and Qiu [3] is within the framework of control-oriented identification and is not applicable here.

Identification procedure:

1. Design the identification experiment, e.g., the excitation signal u is generated. Many identification techniques or guidelines for a single-rate open-loop identification are

still applicable. A so-called vectorized excitation signal is discussed in [26]: an n-dimensional vector signal whose components are relatively independent is generated first, then is inverse lifted by L_n^{-1} as the excitation signal.

2. Estimate the time delay τ as $kh < \hat{\tau} \leq kh + h$ after collecting and preprocessing the multirate input and output data. Next, shift the data as described in Section 3.2 to preserve the controllability and observability of the lifted system.

3. Based on the shifted data, identify a lifted model $\underline{\hat{G}_d}$ with the causality constraint – a traditional MIMO open-loop identification problem. Passing through model validation, $\underline{\hat{G}_d}$ is expected to be accurate.

4. Extract a fast-rate model from $\underline{\hat{G}_d}$ using the proposed approaches. Since the time delay is estimated within an interval, i.e., $kh < \hat{\tau} \leq kh + h$, we may incorporate a conservative estimate, $\hat{\tau} = kh$, to get the fast-rate model $\hat{G}_d$. Finally, validate $\hat{G}_d$ or repeat above steps until a satisfactory result is achieved.

Example 4.1

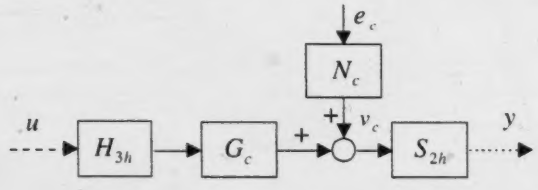

Figure 4.1: Simulation diagram of a SISO MRSD system

For an MRSD system depicted in Figure 4.1, take the process and noise system to be

$$G_c(s) = \frac{1}{20s^2 + 4s + 1} e^{-5s}, \; N_c(s) = \frac{1}{10s + 1},$$

and $m = 3$, $n = 2$, $h = 1$ sec. e_c is a white noise with variance 0.333. The identification procedure is: First, we generate a low frequency random binary signal (RBS) in $[-1, 1]$ as the input signal u; second, we estimate the time delay as $6 < \hat{\tau} \leq 7$, i.e., $k = 6$ in (3.5) and shift the measured input u and output y into u_s and y_s, as described in Example 3.1; third, we lift u_s by L_2 and lift y_s by L_3 to form the lifted signals with a time delay no larger than h; next, based on the lifted signals, we choose a 2nd-order lifted model $\underline{\hat{G}_d}$ and compute a fast-rate model with period h; finally, the estimated time delay 6 sec is incorporated to get $\hat{G}_d$. Figure 4.2 compares the step responses of the actual system G_d and the estimated

fast-rate models $\hat{G}_d$, obtained through the proposed approaches: the controllability and observability approach, the matrix roots approach and the frequency-domain approach. All of them achieve satisfactory results.

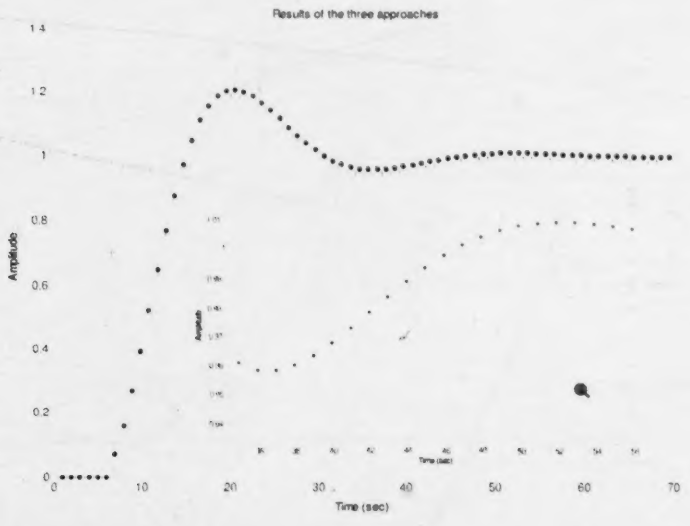

Figure 4.2: Step responses of the actual system (solid) and the estimated fast-rate models by the controllability and observability approach (dash), the matrix roots approach (dotted), and the frequency-domain approach (circle)

Usually, the matrix roots approach gives the best estimation, since the other two require some approximations, e.g., those introduced by model reduction in the frequency-domain approach and by pseudo-inverse in the controllability and observability approach. However, it needs a condition that $\underline{A}$ is diagonalizable to be fulfilled, which limits its application.

Example 4.2

An experiment[2] is implemented on a pilot-scale process in the Computer Process Control laboratory at the University of Alberta. It is a SISO system with the manipulated input u as the cold water valve position and the measured output y as the tank water level, whose time constant is estimated around 400 sec. u and y are represented by currents (mA), which have linear relationships with the physical units. Around an operating point $u = 11$ mA and $y = 10.3$ mA, a low frequency RBS input with a limiting magnitude of 0.4 mA, a constraint

[2]Data and Matlab programs are available online: http://www.ee.ualberta.ca/~jwang/paper.html.

for safety, is designed. The input updating period is 80 sec and the output sampling period is 120 sec. Thus, $m = 2$, $n = 3$ and $h = 40$ sec, a dual configuration to Example 4.1. With "cheap" data acquisition, we simultaneously measure the input and output every 40 sec, say, u_f and y_f, besides collecting the multirate data u and y. Following a similar procedure as that in Example 4.1, we estimate a 2nd-order fast-rate model with period 40 sec, using the matrix roots approach. To validate the model, we take u_f as the input and estimate the model output, which is compared with the measured fast-rate output y_f in Figure 4.3. The model captures the process dynamics and steady states very well.

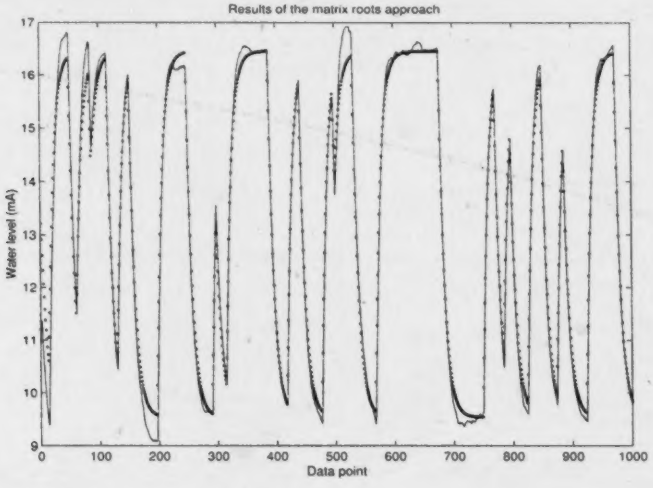

Figure 4.3: Comparison of the measured water level (solid) and the estimated water level (dotted)

Chapter 5

Noise Model and MIMO MRSD Systems

Up to now, we have finished the discussion for SISO MRSD systems using the output error model structure. This chapter serves as an extention in two aspects: Is it possible to get the fast-rate noise system? How about the extension into MIMO cases? The following discussion will show that the discrete-time noise system with period h is not always reachable; extension into MIMO MRSD systems is straightforward under a new interpretation of coprimeness and trouble-free time delays.

5.1 Noise Model Discussion

In the previous chapters, we adopt an output error model structure to describe the lifted system and represented it in an innovation form of a state-space model with $\underline{K} = 0$:

$$\dot{x} = \underline{A}\,x + \underline{B}\,\underline{u} + \underline{K}\,\underline{e}, \tag{5.1a}$$

$$\underline{y} = \underline{C}\,x + \underline{D}\,\underline{u} + \underline{e}. \tag{5.1b}$$

If $\underline{K} \neq 0$, a lifted noise system will be estimated simultaneously. Is it possible to obtain the discrete-time noise system with period h from the estimated lifted noise system? To answer the question, we start with a configuration in Figure 5.1. Since y is sampled with period nh, we need to fictitiously sample the continuous-time white noise e_c with the same period into e. Next, we lift y by L_m, which implies that the noise system also needs to be lifted. Thus, we have a discrete-time noise system with period nh: $N_{nh} := S_{nh} N_c H_{nh}$ and a lifted noise system with period mnh: $\underline{N_{nh}} := L_m N_{nh} L_m^{-1}$ (See Figure 5.2). Note that the noise loop is not a multirate system, but a single-rate one. Therefore, we have an overall

LTI system

$$\underline{y} = \underline{G_d}\,\underline{u} + \underline{N_{nh}}\,\underline{e}.$$

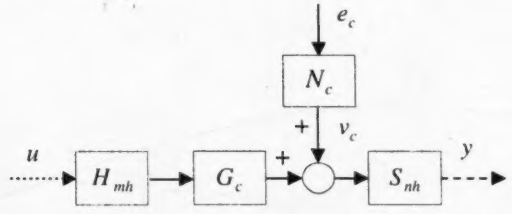

Figure 5.1: Block diagram of a SISO MRSD system with a noise system

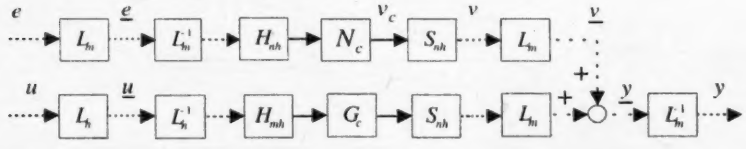

Figure 5.2: The lifted SISO MRSD system with a noise system

Now, let us investigate the possibility of obtaining a discrete-time noise system $N_h := S_h N_c H_h$ with period h after $\underline{N_{nh}}$ has been estimated. If N_h has a state-space representation

$$D_N + C_N\,(zI - A_N)^{-1}\,B_N =: \left[\begin{array}{c|c} A_N & B_N \\ \hline C_N & D_N \end{array}\right], \tag{5.2}$$

then, by the definition of step-invariant-transformation, N_{nh} can be represented as

$$\left[\begin{array}{c|c} A_{N_nh} & B_{N_nh} \\ \hline C_{N_nh} & D_{N_nh} \end{array}\right] := \left[\begin{array}{c|c} A_N^n & B_N + A_N B_N + \cdots + A_N^{n-1} B_N \\ \hline C_N & D_N \end{array}\right]. \tag{5.3}$$

The transfer matrix of $\underline{N_{nh}}$ is [21]

$$\left[\begin{array}{c|c} \underline{A_N} & \underline{B_N} \\ \hline \underline{C_N} & \underline{D_N} \end{array}\right] := \left[\begin{array}{c|ccc} A_{N_nh}^m & A_{N_nh}^{m-1} B_{N_nh} & A_{N_nh}^{m-2} B_{N_nh} & \cdots & B_{N_nh} \\ \hline C_{N_nh} & D_{N_nh} & 0 & \cdots & 0 \\ C_{N_nh} A_{N_nh} & C_{N_nh} B_{N_nh} & D_{N_nh} & \cdots & 0 \\ \vdots & \vdots & \vdots & \ddots & \vdots \\ C_{N_nh} A_{N_nh}^{m-1} & C_{N_nh} A_{N_nh}^{m-2} B_{N_nh} & C_{N_nh} A_{N_nh}^{m-3} B_{N_nh} & \cdots & D_{N_nh} \end{array}\right]. \tag{5.4}$$

If $A_N = A$, i.e., the noise system has the same dynamics as the process, $\underline{A}$, $\underline{B}$, $\underline{C}$ and $\underline{D}$ in (5.1) will have the structures in (2.7). The estimation of $\underline{G_d}$ will be the same as that using the output error model structure. Comparing (5.4) with (5.1), we have

$$\underline{A_N} = \underline{A},\ \underline{B_N} = \underline{K},\ \underline{C_N} = \underline{C},\ \underline{D_N} = I. \tag{5.5}$$

Thus, A_{N_nh}, B_{N_nh}, C_{N_nh} and D_{N_nh} can be computed from (5.4) and (5.5). Next, $A_N = A$, $D_N = I$, B_N and C_N can be extracted from (5.3). On the other hand, if $A_N \neq A$, new states will be introduced. The complexity increases dramatically and it is hard for $\underline{\hat{G}_d}$ and $\underline{\hat{N}_{nh}}$ to preserve structures shown in (2.7) and in (5.4), respectively. Even if $\underline{\hat{N}_{nh}}$ does achieve such a structure, it will generally reach N_{nh} only, since the mapping from N_{nh} to N_h is not one-to-one.

5.2 Extension into MIMO MRSD Systems

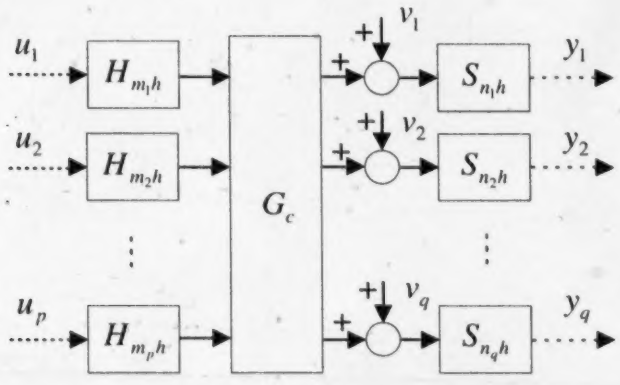

Figure 5.3: A general MIMO MRSD system

In this section, we consider a general MIMO MRSD system depicted in Figure 5.3 that has p inputs and q outputs with different sampling rates. Is it possible to get a discrete-time fast-rate MIMO system with the base period h? From Proposition 1, we conclude that a fast-rate system with period h is possible to be obtained uniquely if and only if (m_i, n_j) are coprime for all i and j. The output and input signals will be lifted by L_{J/n_j} and L_{J/m_i}, respectively, where J is the least common multiple of $(m_1, m_2, \cdots, m_p, n_1, n_2, \cdots, n_q)$. Similar as in the SISO case, the lifted system can be shown to be an LTI system with the sampling period Jh.

What are the new challenges? Most results in the SISO case can be extended into MIMO systems with minor modifications, e.g., increased dimensions and more complicated structures. However, the time-delay problem becomes difficult. The data shifting is not always feasible, although time delays of an MIMO system can be estimated in the same way as that of a SISO system. Therefore, the extension will be confined to a class of MIMO MRSD systems, where

1. (m_i, n_j) are coprime for all i and j. Note that any common factor of them can be sorbed into h;

2. Data shifting for the time-delay problem is feasible. In fact, it is not a must-satisfied condition, since the purpose of data shifting is to preserve the controllability and observability of the lifted system that is only a sufficient condition for identifiability.

In the following, we take an MISO MRSD system, which satisfies the above conditions, as an example to illustrate the extension. Doing so will not loss generality, since an MIMO system is indeed a set of MISO systems.

Example 5.1

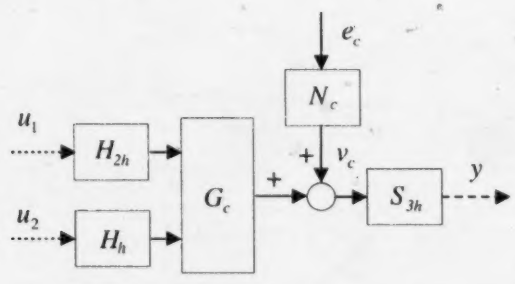

Figure 5.4: Simulation diagram of an MISO MRSD system

For a system depicted in Figure 5.4 where $G_c = [G_1\ G_2]$, take the process and noise system to be

$$G_1 = \frac{1}{20s^2 + 4s + 1} e^{-5s},\ G_2 = \frac{1}{20s + 1} e^{-5s},\ N_c(s) = \frac{1}{10s + 1}.$$

The noise source e_c is a white noise with variance 0.333. Here $m_1 = 2$, $m_2 = 1$, $n = 3$ and $h = 1$ sec. Both (m_1, n) and (m_2, n) are coprime. The least-common-multiple is 6. We lift u_1 by L_3 into $\underline{u_1}$, u_2 by L_6 into $\underline{u_2}$ and y by L_2 into $\underline{y}$, as depicted in Figure 5.5. Thus, $\underline{u_1}$, $\underline{u_2}$ and $\underline{y}$ share the same period 6 sec, and form a discrete-time LTI system $\underline{G_d}$. If our objective, $G_d := S_h G_c H_h$, has a state-space representation

$$\left[\begin{array}{c|cc} A & B_1 & B_2 \\ \hline C & D_1 & D_2 \end{array}\right],$$

then, the lifted system $\underline{G_d}$ is

$$\left[\begin{array}{c|cc} \underline{A} & \underline{B} \\ \hline \underline{C} & \underline{D} \end{array}\right] := \left[\begin{array}{c|cccccccccc} A^6 & \left(A^5 + A^4\right) B_1 & \left(A^3 + A^2\right) B_1 & (A + I) B_1 & A^5 B_2 & A^4 B_2 & A^3 B_2 & A^2 B_2 & AB_2 & B_2 \\ C & D_1 & 0 & 0 & D_2 & 0 & 0 & 0 & 0 & 0 \\ CA^3 & C\left(A^2 + A\right) B_1 & CB_1 + D_1 & 0 & CA^2 B_2 & CAB_2 & CB_2 & D_2 & 0 & 0 \end{array}\right]. \quad (5.6)$$

The causality constraint, i.e., $\underline{D}$ is block lower triangular, can be preserved after some coordinate transformations [4]. However, for identification purpose, it is not necessary to do so as long as the estimates of the matrices $\underline{A}$, $\underline{B}$, $\underline{C}$ and $\underline{D}$ have the required structures in (5.6).

The identification procedure is similar to that in the SISO case. First, we generate two low frequency RBS signals in $[-1, 1]$ as the input signals u_1 and u_2. Second, correlation analysis gives a time-delay matrix for u_1 and y

$$\Gamma_1 = \begin{bmatrix} 2 & 2 & 2 \\ 1 & 1 & 2 \end{bmatrix}$$

and another for u_1 and y

$$\Gamma_2 = \begin{bmatrix} 1 & 2 & 2 & 2 & 2 & 2 \\ 1 & 1 & 1 & 1 & 2 & 2 \end{bmatrix}.$$

The time delay between u_1 and y is estimated as $6 < \hat{\tau}_1 \leq 7$ and that between u_2 and y is $5 < \hat{\tau}_2 \leq 6$. The two inequalities give

$$6 = 2k_1 + 3k_2, \; 5 = k_3 + 3k_2.$$

If $k_1 = 3$, $k_2 = 0$, and $k_3 = 5$, we keep y unchanged as y_s, and shift u_1, u_2 by time advancing by 3 samples and 5 samples, respectively, i.e., $u_{1s}[l] = u_1[l+3]$, $u_{2s}[l] = u_2[l+5]$. Third, we lift u_{1s} by L_3, u_{2s} by L_6 and y_s by L_3 to form the lifted signals with time delays no larger than h. Next, based on the lifted signals, we estimate a lifted model $\underline{\hat{G}_d}$ and compute a fast-rate model with period h. Finally, the estimated time delays $\tau_1 = 6$ sec and $\tau_2 = 5$ sec are incorporated to get $\hat{G}_d$. Figures 5.6 and 5.7 compare the step responses and Bode plots of the actual system G_d and the estimated fast-rate model $\hat{G}_d$ obtained by the matrix roots approach. A good estimation is achieved. However, comparing to the SISO case, one of the drawbacks of the lifting technique becomes more obvious, i.e., the dimension of the lifted system is usually large, which increases the burden of identification.

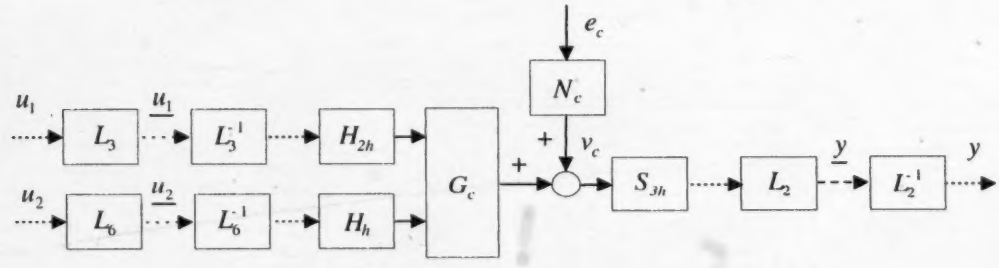

Figure 5.5: The lifted MISO MRSD system

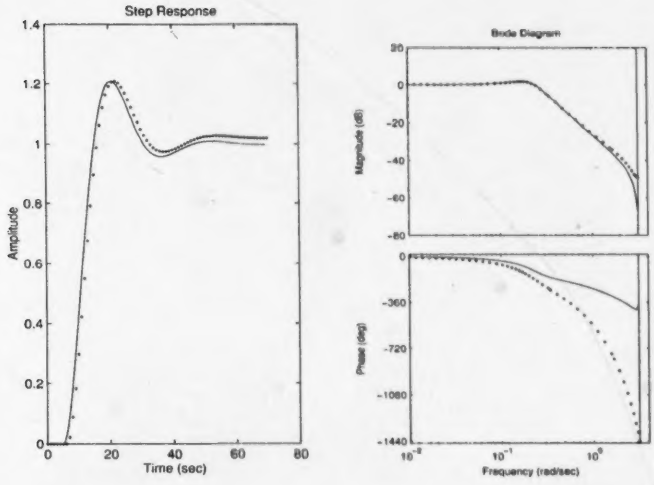

Figure 5.6: Step responses and Bode plots of actual system G_{d1} from u_1 to y (solid) and the estimated model $\hat{G}_{d1}$ (dotted)

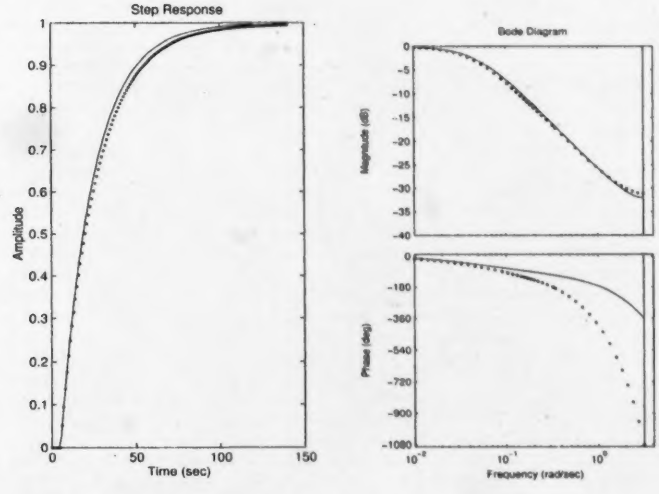

Figure 5.7: Step responses and Bode plots of actual system G_{d2} from u_2 to y (solid) and the estimated model $\hat{G}_{d2}$ (dotted)

Chapter 6

Fast-Sampling Direct Identification of Closed-Loop Systems

This chapter studies the second problem, identification of closed-loop systems without external excitation using a so-called fast-sampling direct approach. It will be shown that an external persistently exciting (PE) signal is no longer a necessary condition for identification in a closed-loop system with linear output feedback. Based on the frequency-domain identifiability analysis, the proposed approach is further investigated and evaluated by simulation.

6.1 Introduction

As an important part in the system identification field, identification of closed-loop systems has long been of prime interest both in academic research and in industrial application for many reasons. It may due to physical constraints, e.g., inherent feedback mechanisms exist, or the open-loop system is unstable and has to be controlled for production or safety reasons. In some cases, it owes to the purposes of identification, e.g., if a linearized dynamic model around a nominal operation point is desired for control, then it is natural and beneficial to achieve this by closed-loop identification [18]. Moreover, if there are constraints in the input/output variance, it would be better to implement identification using closed-loop experiments [15].

A wide variety of approaches have been studied in numerous references and conventionally categorized into three groups: the direct approach, the indirect approach, the joint input-output approach [29, 12]. Their properties, e.g., advantages and drawbacks, have been studied thoroughly in [12]. The direct approach, applied using the prediction error method (PEM), is regarded as a prime choice for its simplicity and optimality, to which our

approach belongs.

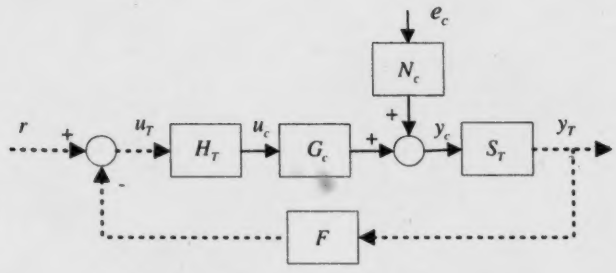

Figure 6.1: Block diagram of a typical closed-loop system

One of the kernel topics in identification of closed-loop systems is identifiability. Figure 6.1 depicts a typical SISO closed-loop system, where G_c is a continuous-time LTI and causal process; N_c is a continuous-time LTI noise system; F is a discrete-time LTI controller; H_T is a zero-order hold with period T; S_T is a sampler with period T. For such a system, the identification objective is to estimate a discrete-time model of $G_T := S_T G_c H_T$. It is well-known that identifiability is ensured by adding an external PE test signal [17], e.g., the reference signal r. Note that the PE signal can be equivalently entered at other points. However, adding such a signal sometimes is undesirable, since it usually disturbs the normal operation and affects product qualities. Is it possible to achieve identifiability without external excitation? A positive answer was given by a so-called output intersampling approach [39, 40]. The approach, called as the fast-sampling direct approach in our context,[1] is a simple modification of the traditional direct approach.

> For a closed-loop system depicted in Figure 6.1, the output y_c is fast-sampled with period $h := T/P$ into y, where P is a positive integer. A fast-sampled version of the input u_c, say u, with period h is also available from the known control input u_T because of the zero-order hold. Based on the fast-rate signals y and u, applying the traditional direct approach gives a fast-rate process model $\hat{G}_h$ with period h, i.e., an estimate of $G_h := S_h G_c H_h$. $\hat{G}_h$ can uniquely determine a slow-rate process model $\hat{G}_T$ with T, namely, the identification objective.

In [40] identifiability was proven to be achieved by analyzing details of the identification algorithms, e.g., Jacobian and Hessian of the prediction error. However, the analysis therein is inordinately complicated and incapable of explaining some phenomena met in simulation.

[1] We feel that the name is more transparent than the output intersampling approach, even though the idea is same.

Our purpose of this work is to provide an instructive and insightful view to answer the following questions:

- Does the fast-sampling direct approach give a model $\hat{G}_T$ such that $\hat{G}_T = G_T$ as the data length goes to infinity, if $r = 0$?
- What are properties of the proposed approach, such as advantages and drawbacks?

The rest of the chapter is organized as follows. To give a clear background, we review the concept of identifiability and a fundamental equation in Section 6.2. Section 6.3 proposes a basic idea guiding the subsequent identifiability analysis. Section 6.4 shows that the fast-sampling direct approach brings LPTV systems on the stage. Next, the prediction error is proven to be nonstationary in Section 6.5. To describe statistical properties of such a nonstationary signal, bifrequency maps and bispectra are introduced in Section 6.6. Using these tools, identifiability of the proposed approach is analyzed in Section 6.7. Finally, Section 6.8 evaluates the proposed approach by simulation examples.

6.2 Preliminary

Since the terminology "identifiability" and a fundamental equation will be used extensively, it is worthy to introduce them in details. First, we quote some words about identifiability from a celebrated book [29]:

> Identifiability is a concept that is central in identification problems. Loosely speaking, the problem is whether the identification procedure will yield a unique value of the parameter θ, and/or whether the resulting model is equal to the true system. $\cdots$. The issue involves aspects on whether the data set (the experimental condition) is informative enough to distinguish between different models as well as properties of the model structure itself $\cdots$

Henceforth, we interpret "identifiability" simply as a concept of whether the resulting model is equal to the true system and assume that other aspects, e.g., the model structure, satisfy the required conditions and do not cause difficulty in obtaining the true system. The concept that two systems $G_1(z)$ and $G_2(z)$ are equal is defined as $G_1(e^{j\omega}) = G_2(e^{j\omega})$ for almost all ω. Since in the fast-sampling direct approach G_T is obtained by estimating G_h, the identifiability question can be rephrased as: If $r = 0$, does the fast-sampling direct approach give a fast-rate model $\hat{G}_h$ such that $\hat{G}_h = G_h$ as the data length N goes to infinity?

Second, we introduce a fundamental equation. If the true system is

$$y(t) = G_0(z)u(t) + N_0(z)e(t),$$

we estimate G_θ and N_θ in

$$y(t) = G_\theta(z)u(t) + N_\theta(z)e(t)$$

by minimizing the prediction error ε defined as

$$\tilde{\varepsilon}(t,\theta) = N_\theta^{-1}[(G_0 - G_\theta)\,u(t) + N_0\,e(t)]. \tag{6.1}$$

If the PEM is used with the most-common criterion

$$\hat{\theta}_N = \arg\min_\theta \frac{1}{N}\sum_{t=1}^{N}\frac{1}{2}\varepsilon^2(t,\theta), \tag{6.2}$$

we have a frequency-domain description of the estimation of parameters θ as the data length N goes to infinity [41]:

$$\begin{aligned}\hat{\theta} \;=\; \arg\min_\theta \frac{1}{4\pi}\int_{-\pi}^{\pi}\Bigg\{ & \frac{\left|G_0\left(e^{j\omega}\right) + B_\theta\left(e^{j\omega},\theta\right) - G_\theta\left(e^{j\omega},\theta\right)\right|^2 \Phi_u\left(e^{j\omega}\right)}{\left|N_\theta\left(e^{j\omega},\theta\right)\right|^2} \\ & + \frac{\left|N_0\left(e^{j\omega}\right) - N_\theta\left(e^{j\omega},\theta\right)\right|^2\left(\lambda - \frac{\left|\Phi_{ue}\left(e^{j\omega}\right)\right|^2}{\Phi_u\left(e^{j\omega}\right)}\right)}{\left|N_\theta\left(e^{j\omega},\theta\right)\right|^2} + \lambda\Bigg\}\mathrm{d}\omega,\end{aligned} \tag{6.3}$$

where

$$B_\theta\left(e^{j\omega},\theta\right) = \frac{\left[N_0\left(e^{j\omega}\right) - N_\theta\left(e^{j\omega},\theta\right)\right]\Phi_{eu}\left(e^{j\omega}\right)}{\Phi_u\left(e^{j\omega}\right)}. \tag{6.4}$$

Here λ is the variance of the discrete-time white noise e; $\Phi_u(e^{j\omega})$ is the power spectrum of the discrete-time input signal u

$$\Phi_u(e^{j\omega}) = \sum_{\tau=-\infty}^{\infty} R_u(\tau)\,e^{-i\tau\omega},$$

where

$$R_u(\tau) = \overline{E}[u(t)\,u(t-\tau)] = \lim_{N\to\infty}\frac{1}{N}\sum_{t=1}^{N}E[u(t)\,u(t-\tau)];$$

$\Phi_{eu}(e^{j\omega})$ and $\Phi_{ue}(e^{j\omega})$ are the cross spectra of u and e, e.g.,

$$\Phi_{ue}(e^{j\omega}) = \sum_{\tau=-\infty}^{\infty} R_{ue}(\tau)\,e^{-i\tau\omega},$$

where

$$R_{ue}(\tau) = \overline{E}[u(t)\,e(t-\tau)] = \lim_{N\to\infty}\frac{1}{N}\sum_{t=1}^{N}E[u(t)\,e(t-\tau)].$$

Such spectra are defined for the so-called Quasi-Stationary signals [29] and can be understood as limit values of the conventional spectra of stochastic signals.

6.3 A Basic Idea

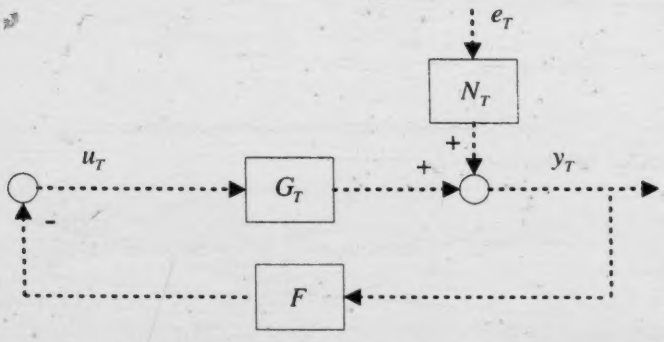

Figure 6.2: Traditional direct approach in a closed-loop system without external excitation

First, let us investigate the reason that identifiability is lost for the traditional direct approach if there is no external excitation. If $r = 0$, Figure 6.1 is simplified into Figure 6.2, where N_T is the discrete-time counterpart of N_c with period T, i.e., $N_T := S_T N_c H_T$ and the continuous-time white noise e_c are fictitiously sampled into e_T with period T, the same sampling period as that of y_T. Two equations exist

$$y_T = G_T \cdot u_T + N_T \cdot e_T \tag{6.5}$$

$$u_T = -F \cdot y_T \tag{6.6}$$

If the traditional direct approach is applied to y_T and u_T, identification likely converges to (6.6) instead of (6.5), since the former is noise-free. Such a viewpoint can be formally captured by analyzing the fundamental equation (6.3). The transfer function from e_T to u_T is

$$u_T = -FS_0N_T \cdot e_T, \tag{6.7}$$

where S_0 is the sensitivity function, $S_0 := (1 + G_T F)^{-1}$. Since F, S_0 and N_T are LTI systems, we have [29]

$$\Phi_{u_T} = |FS_0N_T|^2 \lambda_T, \ \Phi_{u_T e_T} = -(FS_0N_T)\lambda_T, \tag{6.8}$$

where λ_T is the variance of e_T. Thus, the second weighting term in (6.3) becomes

$$\lambda_T - \frac{|\Phi_{u_T e_T}|^2}{\Phi_{u_T}} = \lambda_T - \frac{|FS_0N_T|^2 \lambda_T^2}{|FS_0N_T|^2 \lambda_T} = 0, \tag{6.9}$$

which implies that if $N_T \neq 1$, in general $\hat{N}_T \neq N_T$ and $\hat{G}_T \neq G_T$ (for $B_\theta \neq 0$ in (6.4)), i.e., identifiability is lost.

Now, if the fast-sampling direct approach is applied, it is shown later that there is an LPTV controller instead of an LTI one in (6.6). Intuitively, an LPTV controller brings a possibility that identification could converge to an equation like (6.5), because data are going to be fitted by an LTI model. This is analogous to the shifting between different linear regulators in [29].

An Basic Idea

Fast-sampling direct approach brings an LPTV controller, which implies that the relations in (6.8) and (6.9) no longer hold. Thus, our analysis is going to update these relations and show a non-zero weighting term.

The analysis consists of four steps discussed in the subsequent sections:

- Use the lifting technique to find the LPTV systems;
- Check stationarity of the prediction error;
- Introduce bifrequency maps and bispectra;
- Analyze identifiability of the proposed approach.

6.4 Lifting Technique in the Closed-Loop System

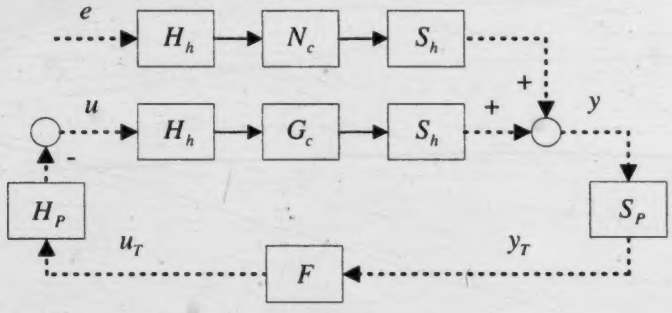

Figure 6.3: A closed-loop system with multirate blocks

In order to make a similar analysis as (6.9), we need to find the relation between the fast-rate input and the fast-rate white noise, which can be obtained by the lifting technique in several steps. Other methods might be able to do this; however, using the lifting technique is clear and systematic.

Step 1: From $T = Ph$ and properties $S_T = S_P S_h$, $H_T = H_h H_P$, where S_P is the discrete-time down-sampler by a factor of P (see (2.3)) and H_P is the discrete-time zero-order hold by a factor of P (see (2.4)), we get Figure 6.3 from Figure 6.1 if $r = 0$. Here e_c is fictitiously sampled with period h into e; u is the fast-rate control input with period h; y is the fast-rate output with period h. Thus, we have a fast-rate process $G_0 := G_h = S_h G_c H_h$ and a fast-rate noise system $N_0 := N_h = S_h N_c H_h$,[2] both with period h. Note that multirate signals, e.g., y and y_T, u and u_T, coexist in Figure 6.3.

Step 2: By properties $L_P L_P^{-1} = I$ and $L_P^{-1} L_P = I$, we have Figure 6.4 that is equivalent to Figure 6.3.

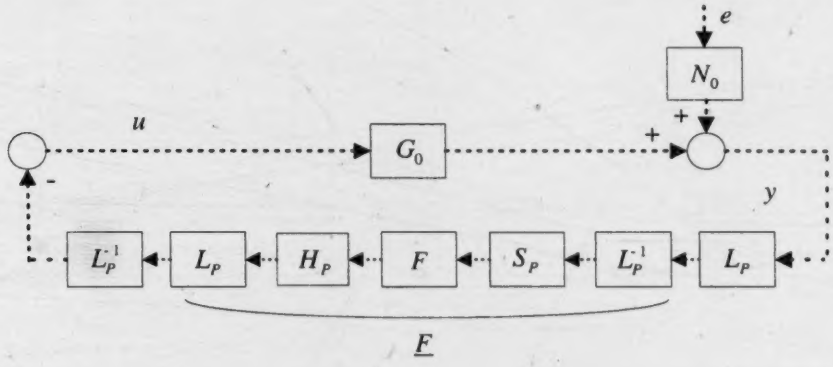

Figure 6.4: A lifted closed-loop system No.1

Fact 1 $\underline{F} := L_P H_P F S_P L_P^{-1}$ *is a P-input and P-output LTI system; it has a state-space representation*

$$\left[\begin{array}{c|c} \underline{A} & \underline{B} \\ \hline \underline{C} & \underline{D} \end{array}\right] := \left[\begin{array}{c|cccc} A & B & 0 & \cdots & 0 \\ \hline C & D & 0 & \cdots & 0 \\ C & D & 0 & \cdots & 0 \\ \vdots & \vdots & \vdots & \ddots & \vdots \\ C & D & 0 & \cdots & 0 \end{array}\right],$$

if F *is represented by* $\left[\begin{array}{c|c} A & B \\ \hline C & D \end{array}\right]$.

Proof: To prove that $\underline{F}$ is LTI, it suffices to show that $U^* \underline{F} U = U$, where U^* and U are the discrete-time unit time-advance and time-delay operators, respectively (see Chapter 2). By properties

$$U^* L_P = L_P (U^*)^P, \; L_P^{-1} U = U^P L_P^{-1},$$

[2]Using notations G_0 and N_0 is to be consistent with those in (6.3).

$$(U^*)^P H_P = H_P U^*,\ S_P U^P = U S_P,$$

we have

$$\begin{aligned} U^* \underline{F} U &= U^* L_P H_P F S_P L_P^{-1} U \\ &= L_P (U^*)^P H_P F S_P U^P L_P^{-1} \\ &= L_P H_P U^* F U S_P L_P^{-1} \\ &= L_P H_P F S_P L_P^{-1} \\ &= \underline{F}. \end{aligned}$$

The transfer matrix of $\underline{F}$ follows from the facts that the transfer matrices of $L_P H_P$ and $S_P L_P^{-1}$ are $\begin{bmatrix} I & I & \cdots & I \end{bmatrix}^T$ and $\begin{bmatrix} I & 0 & \cdots & 0 \end{bmatrix}$, respectively, which are obtained from their physical meanings. □

Note that $H_P F S_P$ is shown to be P-periodic in the proof. In other words, there is an LPTV controller between y and u introduced by the fast-sampling direct approach.

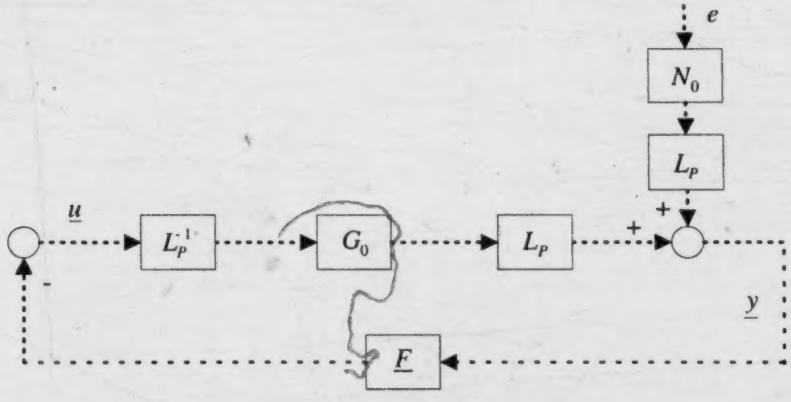

Figure 6.5: A lifted closed-loop system No.2

Step 3: Based on Figure 6.4, we consecutively find its equivalents, Figures 6.5 and 6.6, where $\underline{G_0} := L_P G_0 L_P^{-1}$, $\underline{N_0} := L_P N_0 L_P^{-1}$, i.e., $\underline{G_0}$ and $\underline{N_0}$ are LTI lifted systems [21] and $\underline{u} = L_P \cdot u$, $\underline{y} = L_P \cdot y$ and $\underline{e} = L_P \cdot e$ are lifted signals (see Theorem 8.2.1 in [5]). Therefore, we form an LTI closed-loop system depicted within the dash-dot rectangle in Figure 6.6. There are two equations

$$\underline{y} = \underline{G_0} \cdot \underline{u} + \underline{N_0} \cdot \underline{e}, \tag{6.10}$$

$$\underline{u} = -\underline{F} \cdot \underline{y}. \tag{6.11}$$

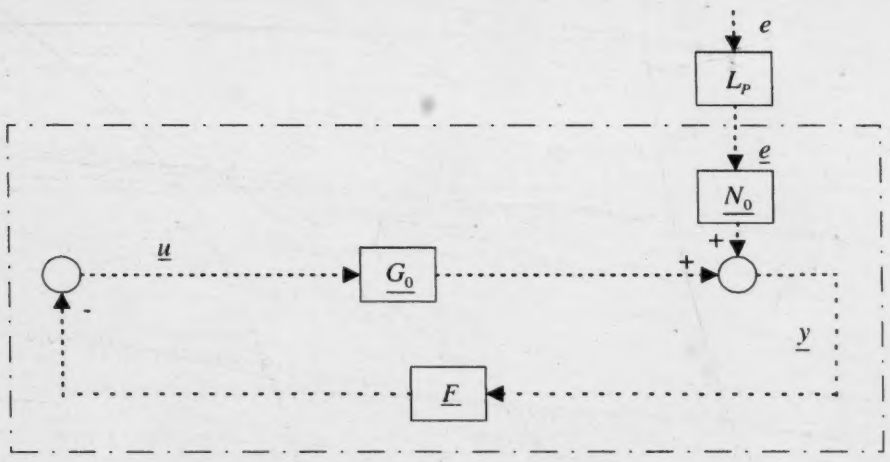

Figure 6.6: A lifted closed-loop system No.3

From (6.10) and (6.11), we obtain the transfer function between $\underline{u}$ and $\underline{e}$

$$\underline{u} = -\underbrace{\underline{F}(I + \underline{G_0}\underline{F})^{-1}\underline{N_0}}_{M} \cdot \underline{e}. \tag{6.12}$$

M has a special transfer matrix

$$M := \begin{bmatrix} M_0 & M_1 & \cdots & M_{P-1} \\ M_0 & M_1 & \cdots & M_{P-1} \\ \vdots & \vdots & & \vdots \\ M_0 & M_1 & \cdots & M_{P-1} \end{bmatrix}, \tag{6.13}$$

where

$$M_i = -F\left[1 + \left(\sum_{j=1}^{P} G_{1,j}\right) F\right]^{-1} N_{1,(i+1)}.$$

Here $G_{1,j}$ and $N_{1,(i+1)}$ are the subsystems of $\underline{G_0}$ and $\underline{N_0}$, respectively,

$$\underline{G_0} = \begin{bmatrix} G_{11} & G_{12} & \cdots & G_{1,P} \\ G_{12} & G_{22} & \cdots & G_{2,P} \\ \vdots & \vdots & & \vdots \\ G_{P,1} & G_{P,2} & \cdots & G_{P,P} \end{bmatrix}, \ \underline{N_0} = \begin{bmatrix} N_{11} & N_{12} & \cdots & N_{1,P} \\ N_{12} & N_{22} & \cdots & N_{2,P} \\ \vdots & \vdots & & \vdots \\ N_{P,1} & N_{P,2} & \cdots & N_{P,P} \end{bmatrix}.$$

Let us see (6.13) by taking $P = 2$ (the general case follows similarly):

$$\begin{aligned} M &= -\underline{F}(I + \underline{G_0}\underline{F})^{-1}\underline{N_0} \\ &= \begin{bmatrix} -F & 0 \\ -F & 0 \end{bmatrix} \left(I + \begin{bmatrix} G_{11} & G_{12} \\ G_{21} & G_{22} \end{bmatrix} \begin{bmatrix} F & 0 \\ F & 0 \end{bmatrix}\right)^{-1} \begin{bmatrix} N_{11} & N_{12} \\ N_{21} & N_{22} \end{bmatrix} \end{aligned}$$

$$
\begin{aligned}
&= \begin{bmatrix} -F & 0 \\ -F & 0 \end{bmatrix} \begin{bmatrix} 1+(G_{11}+G_{12})F & 0 \\ (G_{21}+G_{22})F & 1 \end{bmatrix}^{-1} \begin{bmatrix} N_{11} & N_{12} \\ N_{21} & N_{22} \end{bmatrix} \\
&= \begin{bmatrix} -F & 0 \\ -F & 0 \end{bmatrix} \begin{bmatrix} [1+(G_{11}+G_{12})F]^{-1} & 0 \\ -(G_{21}+G_{22})F[1+(G_{11}+G_{12})F]^{-1} & 1 \end{bmatrix} \begin{bmatrix} N_{11} & N_{12} \\ N_{21} & N_{22} \end{bmatrix} \\
&= \begin{bmatrix} -F[1+(G_{11}+G_{12})F]^{-1}N_{11} & -F[1+(G_{11}+G_{12})F]^{-1}N_{12} \\ -F[1+(G_{11}+G_{12})F]^{-1}N_{11} & -F[1+(G_{11}+G_{12})F]^{-1}N_{12} \end{bmatrix} \\
&=: \begin{bmatrix} M_0 & M_1 \\ M_0 & M_1 \end{bmatrix}, \qquad (6.14)
\end{aligned}
$$

where the fourth equality follows from the matrix inversion identity. Equation (6.13) is a natural result because of the zero-order hold. Equation (6.12) implies that

$$u = \underbrace{L_P^{-1}[-\underline{F}(I+\underline{G_0F})^{-1}\underline{N_0}]L_P}_{M'} \cdot e. \qquad (6.15)$$

Fact 2 *$M' := L_P^{-1}[-\underline{F}(I+\underline{G_0F})^{-1}\underline{N_0}]L_P$ is a P-periodic LPTV system, abbreviated as $(LPTV)_P$.*

Proof: It suffices to show that $(U^*)^P M'U^P = M'$. By properties $(U^*)^P L_P^{-1} = L_P^{-1}U^*$, $L_PU^P = UL_P$ and time invariance of $-\underline{F}(I+\underline{G_0F})^{-1}\underline{N_0}$, we have

$$
\begin{aligned}
(U^*)^P M'U^P &= (U^*)^P L_P^{-1}[-\underline{F}(I+\underline{G_0F})^{-1}\underline{N_0}]L_PU^P \\
&= L_P^{-1}U^*[-\underline{F}(I+\underline{G_0F})^{-1}\underline{N_0}]UL_P \\
&= L_P^{-1}[-\underline{F}(I+\underline{G_0F})^{-1}\underline{N_0}]L_P \\
&= M'.
\end{aligned}
$$

□

In summary, the relation between u and e is no longer an LTI system as that in (6.7), but an $(\text{LPTV})_P$ system in (6.15). Note that a statement in [40] that parts of u and e work in open loop is incorrect.

6.5 Statistical Analysis of the Prediction Error

The purpose of this section is to show that the prediction error like that in (6.1) is not wide-sense-stationary, which implies that the fundamental equation (6.3) is not applicable to the fast-sampling direct approach. Let us introduce three terms.

A. Wide-Sense-Stationary Signals

A discrete-time signal x is said to be wide-sense-stationary (WSS) if two conditions are true for all integers t and k [35]:

$$E[x(t+k)] = E[x(t)], \qquad (6.16)$$

$$E[x(t)x^{\dagger}(t-k)] \;=\; R_{xx}(k), \tag{6.17}$$

where † means the complex conjugate transposition. Note that x is normally assumed to be zero mean. Conditions in (6.16) and (6.17) are the relaxed definitions of the familiar stationarity that is usually defined in terms of density functions [35].

B. Cyclo-Wide-Sense-Stationary Signals

Let $R_{xx}(t_1, t_2) = E[x(t_1)x^{\dagger}(t_2)]$. A discrete-time signal x is said to be cyclo-wide-sense-stationary (CWSS) with period P, abbreviated as $(\text{CWSS})_P$, if

$$E[x(t+kP)] \;=\; E[x(t)], \tag{6.18}$$

$$R_{xx}(t_1+kP, t_2+kP) \;=\; R_{xx}(t_1, t_2), \tag{6.19}$$

for all integers t_1, t_2 and k [34]. If $P = 1$, then x is WSS. Note that (6.18) and (6.19) could have other forms, e.g., those in [36].

C. Jointly Cyclo-Wide-Sense-Stationary Signals

Two discrete-time signals x and y are said to be jointly cyclo-wide-sense-stationary with period P, denoted as $(\text{JCWSS})_P$, if the vector $\begin{bmatrix} x \\ y \end{bmatrix}$ is $(\text{CWSS})_P$ [1]. If $P = 1$, $(\text{JCWSS})_P$ is synonymous with jointly WSS.

Fact 3 *Let x, y be scalar discrete-time signals, and $\underline{x}$, $\underline{y}$ be the lifted versions of x, y, i.e., $\underline{x} = L_P \cdot x$, $\underline{y} = L_P \cdot y$. Then, x is $(\text{CWSS})_P$ iff $\underline{x}$ is WSS; x is WSS iff $\underline{x}$ is WSS with pseudocirculant power spectrum matrix; x, y are $(\text{JCWSS})_P$ iff $\underline{x}$, $\underline{y}$ are jointly WSS.*

Fact 3 is proven scatteredly in [36] and summarized in [1]. A pseudocirculant matrix often appears in multirate systems [42]. If we take a 3×3 pseudocirculant matrix as an example, it will have a form

$$\begin{bmatrix} P_0(z) & P_1(z) & P_2(z) \\ z^{-1}P_2(z) & P_0(z) & P_1(z) \\ z^{-1}P_1(z) & z^{-1}P_2(z) & P_0(z) \end{bmatrix}.$$

Let us apply these concepts and Fact 3 to analyze the prediction error. If we denote G_θ as the estimate of G_0 and N_θ as the estimate of N_0, the prediction error ε is

$$\varepsilon = N_\theta^{-1}[(G_0 - G_\theta) \cdot u + N_0 \cdot e]. \tag{6.20}$$

From the definitions in (6.16) and (6.17), it can be shown that the lifted version of a WSS signal is WSS. If the white noise e has the power spectrum $\Phi_e(e^{j\omega}) = \lambda_0$, then the lifted

version of e, $\underline{e} = L_P \cdot e$, is a WSS signal with power spectrum

$$\Phi_{\underline{e}}\left(e^{j\omega}\right) = \begin{bmatrix} \lambda_0 & 0 & \cdots & 0 \\ 0 & \lambda_0 & \ddots & \vdots \\ \vdots & \ddots & \ddots & 0 \\ 0 & \cdots & 0 & \lambda_0 \end{bmatrix}_{P\times P}.$$

There is an LTI system M between $\underline{u}$ and $\underline{e}$ in (6.12):

$$\underline{u} = -\underbrace{\underline{F}(I + \underline{G_0 F})^{-1}\underline{N_0}}_{M} \cdot \underline{e}.$$

Since $\underline{e}$ is WSS, $\underline{u}$ is WSS and $\underline{u}$, $\underline{e}$ are jointly WSS. The power spectrum of $\underline{u}$ is readily obtained from

$$\Phi_{\underline{u}}\left(e^{j\omega}\right) = M\left(e^{j\omega}\right)\Phi_{\underline{e}}\left(e^{j\omega}\right)M^{*}\left(e^{j\omega}\right). \tag{6.21}$$

$\Phi_{\underline{u}}\left(e^{j\omega}\right)$ is not pseudocirculant, which can be seen through an example. If $P = 2$, (6.13) gives that $M = \begin{bmatrix} M_0 & M_1 \\ M_0 & M_1 \end{bmatrix}$. From (6.21),

$$\Phi_{\underline{u}}\left(e^{j\omega}\right) = \lambda_0\left(|M_0\left(e^{j\omega}\right)|^2 + |M_1\left(e^{j\omega}\right)|^2\right)\begin{bmatrix} I & I \\ I & I \end{bmatrix}.$$

Note that in our context u and e are scalar signals, and M_1 and M_2 are SISO systems. Clearly, $\Phi_{\underline{u}}\left(e^{j\omega}\right)$ is not pseudocirculant. Applying Fact 3 gives that in general u is $(\mathrm{CWSS})_P$, but not WSS; u and e are $(\mathrm{JCWSS})_P$, but not jointly WSS. Based on these, we reach a conclusion about the prediction error.

Fact 4 *In general, the prediction error ε is $(CWSS)_P$, but not WSS.*

Proof: To see that it is $(\mathrm{CWSS})_P$, we lift signals in the system

$$\varepsilon = N_\theta^{-1}[(G_0 - G_\theta)\cdot u + N_0 \cdot e]$$

by L_P and form a lifted system

$$L_P \cdot \varepsilon = L_P N_\theta^{-1}[(G_0 - G_\theta)L_P^{-1}L_P \cdot u + N_0 L_P^{-1}L_P \cdot e],$$

i.e.,

$$\underline{\varepsilon} = \underbrace{L_P N_\theta^{-1}(G_0 - G_\theta)L_P^{-1}}_{G_1}\cdot\underline{u} + \underbrace{L_P N_0 L_P^{-1}}_{G_2}\cdot\underline{e}.$$

Since G_1 and G_2 are clearly LTI, and $\underline{u}$ and $\underline{e}$ have been shown to be WSS, $\underline{\varepsilon}$ is WSS. Apply Fact 3 gives that ε is $(\mathrm{CWSS})_P$. The fact that ε is not WSS can be easily seen from definitions in (6.16) and (6.17). □

6.6 Bifrequency Maps and Bispectra

To describe statistical properties of nonstationary signals, e.g., u and ε in (6.20), we need new concepts, namely, bifrequency maps and bispectra.[3]

6.6.1 Bifrequency Maps

Let us introduce bifrequency maps that are used to describe characteristics of general linear time-varying (LTV) systems first. Next, we will focus on the bifrequency maps of LPTV systems.

A. Bifrequency Maps of General LTV Systems

A discrete-time LTV system with input x and output y is fully specified in the time domain by a so-called Green's function [9]

$$y(m) = \sum_{n=-\infty}^{\infty} k(m,n)\, x(n). \tag{6.22}$$

Here $k(m,n)$ gives the system response at time m to an impulse at time n (m and n are integers). If the system is LTI, (6.22) is in the familiar convolution form

$$y(m) = \sum_{n=-\infty}^{\infty} k(m)\, x(n-m).$$

Sometimes it is useful [7] to rewrite (6.22) in a form resembling the convolution

$$y(m) = \sum_{n=-\infty}^{\infty} h(m,n)\, x(m-n)$$

or

$$y(m) = \sum_{n=-\infty}^{\infty} h_m(n)\, x(m-n), \tag{6.23}$$

where $h(m,n) = k(m,m-n)$ and $h_m(n) := h(m,n)$. The LTV system is also fully specified in the frequency domain by a so-called bifrequency function [9]

$$Y\left(e^{j\omega'}\right) = \int_{-\pi}^{\pi} K\left(e^{j\omega'}, e^{j\omega}\right) X\left(e^{j\omega}\right) d\omega,$$

where

$$K\left(e^{j\omega'}, e^{j\omega}\right) = \frac{1}{2\pi} \sum_{m=-\infty}^{\infty} \sum_{n=-\infty}^{\infty} k(m,n)\, e^{-j\omega' m} e^{j\omega n}. \tag{6.24}$$

[3] This section is based on the framework developed in [1].

Here $Y\left(e^{j\omega'}\right)$ and $X\left(e^{j\omega}\right)$ are the discrete-time Fourier transformations of y and x, respectively. $K\left(e^{j\omega'}, e^{j\omega}\right)$ describes a mapping of the input frequency ω onto the output frequency ω'. Hence, it is called as a bifrequency map [31].

Cascading two LTV systems with Green's functions $k_1(m,n)$, $k_2(m,n)$ and bifrequency functions $K_1\left(e^{j\omega'}, e^{j\omega}\right)$, $K_2\left(e^{j\omega'}, e^{j\omega}\right)$ respectively in this order gives a new LTV system specified by [7, 9]

$$k(m,n) = \sum_{r=-\infty}^{\infty} k_2(m,r)\, k_1(r,n), \tag{6.25}$$

$$K\left(e^{j\omega'}, e^{j\omega}\right) = \int_{-\pi}^{\pi} K_2\left(e^{j\omega'}, e^{j\omega''}\right) K_1\left(e^{j\omega''}, e^{j\omega}\right) d\omega''. \tag{6.26}$$

B. Bifrequency Maps of LPTV Systems

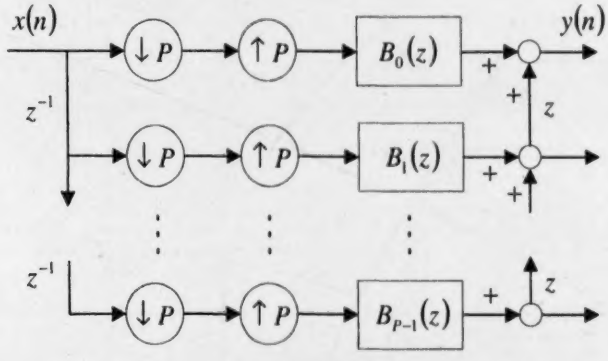

Figure 6.7: Filter bank representation of general LPTV systems

An $(\text{LPTV})_P$ system has a property that $h_m(n)$ in (6.23) is periodic in the output index m with period P, i.e.,

$$h_m(n) = h_{m+P}(n), \text{ for all } m, n.$$

Such an $(\text{LPTV})_P$ system can be always represented as that in Figure 6.7 (see Section 10.1.2 in [42]), where $B_r(z)$ is the transfer function of a scalar LTI system

$$B_r(z) := \sum_{n=-\infty}^{\infty} h_r(n)\, z^{-n}. \tag{6.27}$$

Thus, the $(\text{LPTV})_P$ system is fully characterized by P transfer functions $B_r(z)$. Given a transfer matrix of the lifted version of an $(\text{LPTV})_P$ system such as M in (6.12)

$$M = \begin{bmatrix} M_0 & M_1 & \cdots & M_{P-1} \\ M_0 & M_1 & \cdots & M_{P-1} \\ \vdots & \vdots & & \vdots \\ M_0 & M_1 & \cdots & M_{P-1} \end{bmatrix}, \tag{6.28}$$

we have

$$\begin{aligned} B_0(z) &= \left[1+z^{-1}+z^{-2}+\cdots+z^{-(P-1)}\right] M_0\left(z^P\right), \\ B_1(z) &= \left[1+z^{-1}+z^{-2}+\cdots+z^{-(P-1)}\right] M_1\left(z^P\right), \\ &\vdots \\ B_{P-1}(z) &= \left[1+z^{-1}+z^{-2}+\cdots+z^{-(P-1)}\right] M_{P-1}\left(z^P\right). \end{aligned} \tag{6.29}$$

To see (6.29), we take $P = 2$ (the general case follows similarly). Let M in (6.13) be represented by a state-space model

$$M = \begin{bmatrix} M_0 & M_1 \\ M_0 & M_1 \end{bmatrix} =: \left[\begin{array}{c|cc} A & B_1 & B_2 \\ \hline C & D_1 & D_2 \\ C & D_1 & D_2 \end{array}\right] =: \left[\begin{array}{c|c} \underline{A} & \underline{B} \\ \hline \underline{C} & \underline{D} \end{array}\right].$$

By the transfer matrices of L_2 and L_2^{-1} [5],

$$\begin{aligned} L_2^{-1} M L_2 &= \left[\begin{array}{cc|cc|cc|c} I & 0 & 0 & 0 & 0 & 0 & \cdots \\ \hline 0 & I & 0 & 0 & 0 & 0 & \cdots \\ \hline 0 & 0 & I & 0 & 0 & 0 & \cdots \\ \hline 0 & 0 & 0 & I & 0 & 0 & \cdots \\ \hline 0 & 0 & 0 & 0 & I & 0 & \cdots \\ \hline \vdots & \vdots & \vdots & \vdots & \vdots & \vdots & \end{array}\right] \left[\begin{array}{cccc|c} \underline{D} & 0 & 0 & 0 & \cdots \\ \underline{C}\,\underline{B} & \underline{D} & 0 & 0 & \cdots \\ \underline{C}\,\underline{A}\,\underline{B} & \underline{C}\,\underline{B} & \underline{D} & 0 & \cdots \\ \vdots & \vdots & \vdots & \vdots & \end{array}\right] \left[\begin{array}{cc|cc|cc|c} I & 0 & 0 & 0 & 0 & 0 & \cdots \\ 0 & I & 0 & 0 & 0 & 0 & \cdots \\ \hline 0 & 0 & I & 0 & 0 & 0 & \cdots \\ 0 & 0 & 0 & I & 0 & 0 & \cdots \\ \hline 0 & 0 & 0 & 0 & I & 0 & \cdots \\ 0 & 0 & 0 & 0 & 0 & 0 & \cdots \\ \hline \vdots & \vdots & \vdots & \vdots & \vdots & \vdots & \end{array}\right] \\ &= \begin{bmatrix} D_1 & D_2 & 0 & 0 & 0 & 0 & \cdots \\ D_1 & D_2 & 0 & 0 & 0 & 0 & \cdots \\ CB_1 & CB_2 & D_1 & D_2 & 0 & 0 & \cdots \\ CB_1 & CB_2 & D_1 & D_2 & 0 & 0 & \cdots \\ CAB_1 & CAB_2 & CB_1 & CB_2 & D_1 & D_2 & \cdots \\ CAB_1 & CAB_2 & CB_1 & CB_2 & D_1 & D_2 & \cdots \\ \vdots & \vdots & \vdots & \vdots & \vdots & \vdots & \end{bmatrix}. \end{aligned} \tag{6.30}$$

From (6.30), we obtain two sets of impulse responses

$$\begin{aligned} &\{\ D_1 \quad D_1 \quad CB_1 \quad CB_1 \quad CAB_1 \quad CAB_1 \quad \cdots\ \}, \\ &\{\ D_2 \quad D_2 \quad CB_2 \quad CB_2 \quad CAB_2 \quad CAB_2 \quad \cdots\ \}, \end{aligned}$$

which imply that

$$\begin{aligned} B_0(z) &= D_1 + D_1 z^{-1} + CB_1 z^{-2} + CB_1 z^{-3} + CAB_1 z^{-4} + CAB_1 z^{-5} + \cdots \\ &= \left(D_1 + CB_1 z^{-2} + CAB_1 z^{-4} + \cdots\right) + z^{-1}\left(D_1 + CB_1 z^{-2} + CAB_1 z^{-4} + \cdots\right) \\ &= \left(1 + z^{-1}\right) M_0\left(z^2\right), \end{aligned} \tag{6.31}$$

and similarly,

$$B_1(z) = \left(1 + z^{-1}\right) M_1\left(z^2\right).$$

The purpose of representing an $(\mathrm{LPTV})_P$ system as that in Figure 6.7 is to view it as a maximally decimated filter bank. A P-channel maximally decimated filter bank has a relation between its input x and its output y [42]

$$Y\left(e^{j\omega}\right) = \sum_{q=0}^{P-1} A_q\left(e^{j\omega}\right) X\left(e^{j\left(\omega - \frac{2\pi q}{P}\right)}\right),$$

where

$$A_q\left(e^{j\omega}\right) = \frac{1}{P} \sum_{r=0}^{P-1} H_r\left(e^{j\left(\omega - \frac{2\pi q}{P}\right)}\right) F_r\left(e^{j\omega}\right). \tag{6.32}$$

Here $H_r\left(e^{j\omega}\right)$ is the so-called analysis bank filter and $F_r\left(e^{j\omega}\right)$ is the so-called synthesis bank filter. In Figure 6.7,

$$H_r(z) = z^{-r},\ F_r(z) = z^r B_r(z). \tag{6.33}$$

From (6.32) and (6.33), we have

$$\begin{aligned} A_q\left(e^{j\omega}\right) &= \frac{1}{P} \sum_{r=0}^{P-1} \left(e^{j\left(\omega - \frac{2\pi q}{P}\right)}\right)^{-r} \left(e^{j\omega}\right)^r B_r\left(e^{j\omega}\right) \\ &= \frac{1}{P} \sum_{r=0}^{P-1} e^{j\frac{2\pi q}{P} r} B_r\left(e^{j\omega}\right). \end{aligned}$$

If written in a matrix form,

$$\begin{bmatrix} A_0\left(e^{j\omega}\right) \\ A_1\left(e^{j\omega}\right) \\ \vdots \\ A_{P-1}\left(e^{j\omega}\right) \end{bmatrix} = \frac{1}{P} W_P^{\dagger} \begin{bmatrix} B_0\left(e^{j\omega}\right) \\ B_1\left(e^{j\omega}\right) \\ \vdots \\ B_{P-1}\left(e^{j\omega}\right) \end{bmatrix}, \tag{6.34}$$

where W_P is the Discrete Fourier Transform (DFT) matrix [42]. It is a $P \times P$ symmetric matrix whose entry at the mth row and nth column is equal to $e^{-j\frac{2\pi}{P}mn}$ for $m = 0, 1, \cdots, P-1$ and $n = 0, 1, \cdots, P-1$.

The bifrequency function $K\left(e^{j\omega'}, e^{j\omega}\right)$ of an $(\mathrm{LPTV})_P$ system is also characterized by P functions [1, 31]

$$K\left(e^{j\omega'}, e^{j\omega}\right) = F\left(e^{j\omega'}, e^{j\omega}\right) \sum_{q=-\infty}^{\infty} \delta\left(\omega - \omega' + \frac{2\pi q}{P}\right), \tag{6.35}$$

where $\delta(\cdot)$ is the Dirac-delta function and $F\left(e^{j\omega'}, e^{j\omega}\right)$ is a finite two-dimensional function. Equation (6.35) means that $K\left(e^{j\omega'}, e^{j\omega}\right)$ lies on the lines $\omega - \omega' + \frac{2\pi q}{P} = 0$. On the qth line,

$$F_q\left(e^{j\omega}\right) := F\left(e^{j\omega}, e^{j\left(\omega - \frac{2\pi q}{P}\right)}\right). \tag{6.36}$$

It has been proven in [1] that

$$\begin{aligned} F_q\left(e^{j\omega}\right) &= A_q\left(e^{j\omega}\right), q = 0, 1, \cdots, P-1; \\ F_q\left(e^{j\omega}\right) &= F_{q+P}\left(e^{j\omega}\right) \text{ for all integers } q. \end{aligned} \tag{6.37}$$

In summary, given a lifted version of an $(\text{LPTV})_P$ system represented as (6.28), bispectrum maps (6.35) of the system can be found from (6.37), (6.34) and (6.29).

Example 6.1

For the $(\text{LPTV})_P$ system between u and e in the fast-sampling direct approach, if $P = 2$, its bifrequency maps will have a form as that depicted in Figure 6.8 (the result of Example 6.3). The projection of the bifrequency maps on the ω'-ω plane within a square area $\omega' \in [-\pi, \pi]$, $\omega \in [-\pi, \pi]$ consists of three lines shown in Figure 6.9 (b). If $P = 1$, i.e., an LTI system, the projection has only one line in the area, shown in Figure 6.9 (a). The cases $P = 3$ and $P = 4$ are also shown in Figure 6.9 (c) and (d), respectively.

6.6.2 Bispectra

To describe properties of nonstationary signals as spectra of WSS signals, a few choices exist, e.g., the cyclic spectrum in [14] and the bispectrum in [44]. Here we adopt the latter, for it is geometrically pellucid.

A. Autocorrelation and Bispectrum of a Nonstationary Signal

The autocorrelation $R_x(m, n)$ and bispectrum $\Phi_x\left(e^{j\omega'}, e^{j\omega}\right)$ of a nonstationary signal x are defined as [34]

$$R_x(m, n) = E[x(m)x^\dagger(n)], \tag{6.38}$$

$$\Phi_x\left(e^{j\omega'}, e^{j\omega}\right) = \frac{1}{2\pi} \sum_{m=-\infty}^{\infty} \sum_{n=-\infty}^{\infty} R_x(m, n)\, e^{-j\omega' m} e^{j\omega n}. \tag{6.39}$$

B. Bispectrum of a Cyclo-Wide-Sense-Stationary Signal

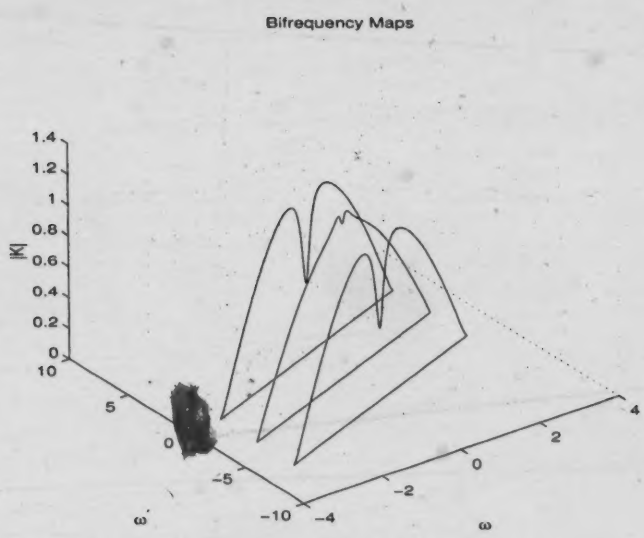

Figure 6.8: Bifrequency maps for $P = 2$

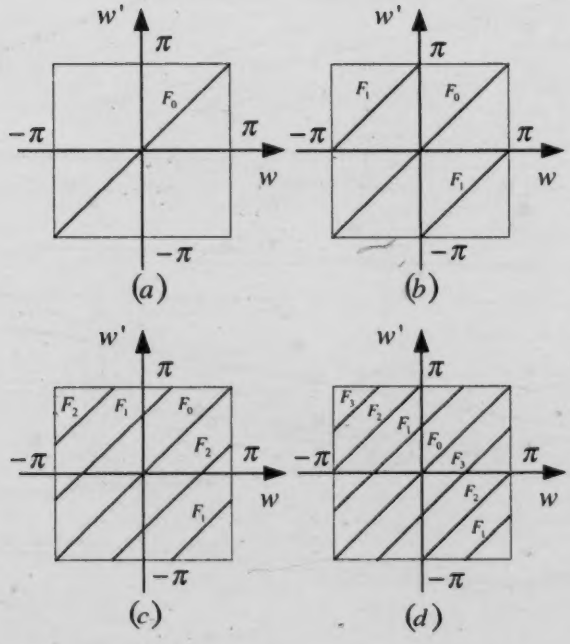

Figure 6.9: Projection of bifrequency maps on the ω'-ω plane: (a) $P = 1$, (b) $P = 2$, (c) $P = 3$, (d) $P = 4$

Analogous to the LPTV system, the bispectrum of a $(\mathrm{CWSS})_P$ signal consists of a set of parallel lines. Indeed, it has very similar expressions provided in [1] as (6.35) and (6.37). Instead of offering those expressions, we will present it later in terms of transformed bispectra through linear systems. In particular, when $P = 1$ and x is a WSS signal with power spectrum $\Phi_x\left(\mathrm{e}^{j\omega}\right)$, its bispectrum is

$$\Phi_x\left(\mathrm{e}^{j\omega'}, \mathrm{e}^{j\omega}\right) = \Phi_x\left(\mathrm{e}^{j\omega}\right) \sum_{q=-\infty}^{\infty} \delta\left(\omega - \omega' + 2\pi q\right). \tag{6.40}$$

Equation (6.40) means that there is only one line in the square area $\omega' \in [-\pi, \pi]$, $\omega \in [-\pi, \pi]$ on the ω'-ω plane (similar to Figure 6.9 (a)).

C. Cross Correlation and Cross Bispectrum of Two Nonstationary Signals

Analogous to (6.38) and (6.39), the cross correlation $R_{yx}(m, n)$ and the cross bispectrum $\Phi_{yx}\left(\mathrm{e}^{j\omega'}, \mathrm{e}^{j\omega}\right)$ of two nonstationary signals x and y are defined as [34]

$$\begin{aligned} R_{yx}(m, n) &= E[y(m)x^{\dagger}(n)], \\ \Phi_{yx}\left(\mathrm{e}^{j\omega'}, \mathrm{e}^{j\omega}\right) &= \frac{1}{2\pi} \sum_{m=-\infty}^{\infty} \sum_{n=-\infty}^{\infty} R_{yx}(m, n)\, \mathrm{e}^{-j\omega' m} \mathrm{e}^{j\omega n}. \end{aligned}$$

6.6.3 Transformation of Bispectra by Linear Systems

It is well known that when a WSS signal x with power spectrum $\Phi_x\left(\mathrm{e}^{j\omega}\right)$ is passed through an LTI system having a stable transfer function $G(z)$, the output y is also a WSS signal with power spectrum [29]

$$\Phi_y\left(\mathrm{e}^{j\omega}\right) = G\left(\mathrm{e}^{j\omega}\right) \Phi_x\left(\mathrm{e}^{j\omega}\right) G^{\dagger}\left(\mathrm{e}^{j\omega}\right),$$

and the cross power spectrum of x and y is

$$\Phi_{yx}\left(\mathrm{e}^{j\omega}\right) = G\left(\mathrm{e}^{j\omega}\right) \Phi_x\left(\mathrm{e}^{j\omega}\right).$$

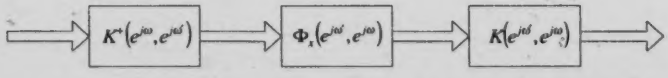

Figure 6.10: Schematic illustration of transformation of bispectra by linear systems.

When a nonstationary signal x with bispectrum $\Phi_x\left(\mathrm{e}^{j\omega'}, \mathrm{e}^{j\omega}\right)$ is passed through an LTV system with bifrequency function $K\left(\mathrm{e}^{j\omega'}, \mathrm{e}^{j\omega}\right)$, the output y is generally nonstationary. Its

bispectrum $\Phi_y\left(e^{j\omega'}, e^{j\omega}\right)$ is the bifrequency function of the cascade shown in Figure 6.10 [1]. Note that Figure 6.10 is a schematic illustration only; it does not mean

$$\Phi_y\left(e^{j\omega'}, e^{j\omega}\right) = K\left(e^{j\omega'}, e^{j\omega}\right)\Phi_x\left(e^{j\omega'}, e^{j\omega}\right)K^{\dagger}\left(e^{j\omega}, e^{j\omega'}\right);$$

instead, (6.26) is applicable. In particular, if the LTV system is an LTI system with transfer function $G(z)$, then according to [1]

$$\Phi_y\left(e^{j\omega'}, e^{j\omega}\right) = G\left(e^{j\omega'}\right)\Phi_x\left(e^{j\omega'}, e^{j\omega}\right)G^{\dagger}\left(e^{j\omega}\right). \tag{6.41}$$

LPTV Systems with WSS Inputs

If an LTV system is $(\text{LTPV})_P$ with bifrequency function $K\left(e^{j\omega'}, e^{j\omega}\right)$ characterized in (6.35) and the input x is WSS with power spectrum $\Phi_x\left(e^{j\omega}\right)$, the bispectrum of the output y is given in [1] as

$$\Phi_y\left(e^{j\omega'}, e^{j\omega}\right) = \sum_{q=0}^{P-1} P_y^q\left(e^{j\omega'}\right)\sum_{m=-\infty}^{\infty}\delta\left(\omega - \omega' + \frac{2\pi q}{P} + 2\pi m\right), \tag{6.42}$$

where

$$P_y^q\left(e^{j\omega'}\right) = \sum_{r=0}^{P-1} F_{r+q}\left(e^{j\left(\omega' + \frac{2\pi q}{P}\right)}\right)F_r^*\left(e^{j\omega'}\right)\Phi_x\left(e^{j\left(\omega' - \frac{2\pi r}{P}\right)}\right).$$

Equation (6.42) means that the bispectrum of y lies on a set of parallel lines

$$\omega - \omega' + \frac{2\pi q}{P} + 2\pi m = 0.$$

The qth line is characterized by $P_y^q\left(e^{j\omega'}\right)$, which is a combination of power spectra of x and its shifted versions. In addition, y is CWSS. To see this, we could use the techniques in Section 6.5 by lifting the LPTV system and applying Fact 3. In general, the output of an LPTV system with a WSS input is CWSS. Similarly, y and x can be shown to be Jointly CWSS.

Fact 5 *The cross bispectra of y and x are*

$$\Phi_{yx}\left(e^{j\omega'}, e^{j\omega}\right) = \sum_{q=0}^{P-1} F_q\left(e^{j\omega}\right)\Phi_x\left(e^{j\left(\omega' - \frac{2\pi q}{P}\right)}, e^{j\omega}\right), \tag{6.43}$$

and

$$\Phi_{xy}\left(e^{j\omega'}, e^{j\omega}\right) = \sum_{q=0}^{P-1}\Phi_x\left(e^{j\omega'}, e^{j\left(\omega - \frac{2\pi q}{P}\right)}\right)F_q^*\left(e^{j\omega}\right). \tag{6.44}$$

Proof: see Appendix B.

Example 6.2

Let us apply (6.42), (6.43) and (6.44) to the LPTV system (6.15) between u and e, where the power spectrum of e is λ_0. If $P = 2$, the bispectrum of u for $\omega' \in [-\pi, \pi]$, $\omega \in [-\pi, \pi]$ is

$$\Phi_u\left(e^{j\omega'}, e^{j\omega}\right) = P_u^0\left(e^{j\omega'}\right)\delta\left(\omega - \omega'\right) + P_u^1\left(e^{j\omega'}\right)\delta\left(\omega - \omega' + \pi\right) + P_u^1\left(e^{j\omega'}\right)\delta\left(\omega - \omega' - \pi\right),$$

where

$$\begin{aligned} P_u^0\left(e^{j\omega'}\right) &= \lambda_0\left[F_0\left(e^{j\omega'}\right)\cdot F_0^*\left(e^{j\omega'}\right) + F_1\left(e^{j\omega'}\right)\cdot F_1^*\left(e^{j\omega'}\right)\right], \\ P_u^1\left(e^{j\omega'}\right) &= \lambda_0\left[F_1\left(e^{j(\omega'+\pi)}\right)\cdot F_0^*\left(e^{j\omega'}\right) + F_0\left(e^{j(\omega'+\pi)}\right)\cdot F_1^*\left(e^{j\omega'}\right)\right]; \end{aligned}$$

the cross bispectra are

$$\begin{aligned} \Phi_{ue}\left(e^{j\omega'}, e^{j\omega}\right) &= \lambda_0 F_0\left(e^{j\omega}\right)\delta\left(\omega - \omega'\right) + \lambda_0 F_1\left(e^{j\omega}\right)\delta\left(\omega - \omega' + \pi\right), \\ \Phi_{eu}\left(e^{j\omega'}, e^{j\omega}\right) &= \lambda_0 F_0^*\left(e^{j\omega}\right)\delta\left(\omega - \omega'\right) + \lambda_0 F_1^*\left(e^{j\omega}\right)\delta\left(\omega - \omega' - \pi\right). \end{aligned}$$

Projections of these bispectra on the ω'-ω plane are shown in Figure 6.11.

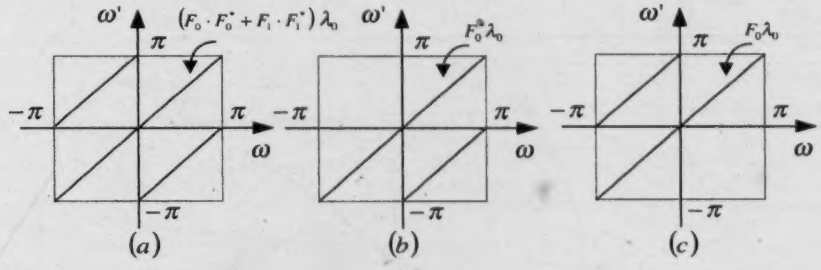

Figure 6.11: Projection of bispectrum and cross bispectra of signals in a closed-loop system: (*a*) Φ_u, (*b*) Φ_{ue}, (*c*) Φ_{eu}

6.7 Identifiability Analysis Using Bispectra

In this section, we derive a frequency-domain expression for the limit loss function, which is a generalized version of (6.3). This expression shows that identifiability is achieved under the fast-sampling direct approach, in three steps.

Step 1: Loss Function for CWSS Prediction Errors

The prediction error ε is shown to be $(\text{CWSS})_P$ in Fact 4. For such a nonstationary signal, we use the autocorrelation in (6.38) and the bispectrum in (6.39) to describe its statistical properties. Since ε is a scalar signal in our context,

$$E\left[\varepsilon^2(t)\right] = E[\varepsilon(t)\varepsilon^\dagger(t)] = R_\varepsilon(t,t). \tag{6.45}$$

Based on the bispectrum of ε

$$\Phi_\varepsilon(e^{j\omega'}, e^{j\omega}) = \frac{1}{2\pi}\sum_{t=-\infty}^{\infty}\sum_{t=-\infty}^{\infty} R_\varepsilon(t,t)\, e^{-j\omega' t} e^{j\omega t},$$

its 2-D inverse Fourier transformation gives [34]

$$R_\varepsilon(t,t) = \frac{1}{2\pi}\int_{-\pi}^{\pi}\int_{-\pi}^{\pi} \Phi_\varepsilon(e^{j\omega'}, e^{j\omega}) e^{j\omega' t} e^{-j\omega t} d\omega d\omega'. \tag{6.46}$$

Note that both R_ε and Φ_ε are functions of θ. If a PEM algorithm (6.2) is used to estimate parameters θ, the loss function as the data length N goes to infinity is [29]

$$\overline{V}(\theta) = \lim_{N\to\infty}\frac{1}{N}\sum_{t=1}^{N}\frac{1}{2}E\left[\varepsilon^2(t)\right].$$

From (6.45) and (6.46), $\overline{V}(\theta)$ can be represented in the frequency domain

$$\begin{aligned}
\overline{V}(\theta) &= \lim_{N\to\infty}\frac{1}{N}\sum_{t=1}^{N}\frac{1}{4\pi}\int_{-\pi}^{\pi}\int_{-\pi}^{\pi}\Phi_\varepsilon(e^{j\omega'}, e^{j\omega}) e^{j\omega' t} e^{-j\omega t} d\omega d\omega' \\
&= \lim_{N\to\infty}\frac{1}{N}\sum_{t=1}^{N}\frac{1}{4\pi}\int_{-\pi}^{\pi}\int_{-\pi}^{\pi}\Phi_\varepsilon(e^{j\omega'}, e^{j\omega}) e^{-j\frac{2\pi q}{P}t} d\omega d\omega', \text{ where } q = 0, 1, \cdots, P-1 \\
&= \lim_{N\to\infty}\frac{1}{N}\sum_{t=1}^{N}\frac{1}{4\pi}\int_{-\pi}^{\pi}\int_{-\pi}^{\pi}\Phi_\varepsilon(e^{j\omega'}, e^{j\omega}) d\omega d\omega', \text{ where } \omega = \omega'.
\end{aligned} \tag{6.47}$$

Here the second equality follows from a fact that the bispectrum of a $(\text{CWSS})_P$ signal lies on the lines $\omega - \omega' = \frac{2\pi q}{P}$, where $q = 0, 1, \cdots, P-1$, and the last equality follows from a property of trigonometry [34]

$$\lim_{N\to\infty}\frac{1}{N}\sum_{t=1}^{N} e^{-j\frac{2\pi q}{P}t} = \begin{cases} 1, & q = 0 \\ 0, & q = 1, 2, \cdots, P-1. \end{cases}$$

Equation (6.47) means that $\overline{V}(\theta)$ only depends on a specific part of $\Phi_\varepsilon(e^{j\omega'}, e^{j\omega})$, i.e., that on the diagonal line $\omega = \omega'$.

Step 2: Bispectrum of the Prediction Error

We now have a characterization of estimation

$$\begin{aligned}\hat{\theta} &= \arg\min_{\theta} \overline{V}(\theta) \\ &= \arg\min_{\theta} \frac{1}{4\pi}\int_{-\pi}^{\pi}\int_{-\pi}^{\pi} \Phi_{\varepsilon}(e^{j\omega'}, e^{j\omega})\mathrm{d}\omega\mathrm{d}\omega', \text{ where } \omega = \omega'. \end{aligned} \tag{6.48}$$

in the frequency domain that is determined by the bispectrum of ε. Let us partition ε into two parts

$$\begin{aligned}\varepsilon &= N_{\theta}^{-1}[(G_0 - G_{\theta})\,u + N_0\,e] \\ &= N_{\theta}^{-1}\left[\begin{array}{cc}(G_0 - G_{\theta}) & (N_0 - N_{\theta})\end{array}\right]\left[\begin{array}{c} u \\ e \end{array}\right] + e. \end{aligned} \tag{6.49}$$

By a standard assumption to avoid algebraic loops [38], the two parts in (6.49) are uncorrelated. Since G_0, G_{θ}, N_0 and N_{θ} are LTI, from (6.41) we have

$$\begin{aligned}\Phi_{\varepsilon}(e^{j\omega'}, e^{j\omega}) &= \frac{1}{N_{\theta}(e^{j\omega'})}\left[\begin{array}{cc} G_0(e^{j\omega'}) - G_{\theta}(e^{j\omega'}) & N_0(e^{j\omega'}) - N_{\theta}(e^{j\omega'})\end{array}\right]\left[\begin{array}{cc}\Phi_u(e^{j\omega'}, e^{j\omega}) & \Phi_{ue}(e^{j\omega'}, e^{j\omega}) \\ \Phi_{eu}(e^{j\omega'}, e^{j\omega}) & \Phi_e(e^{j\omega'}, e^{j\omega})\end{array}\right] \\ &\quad \cdot\left[\begin{array}{c} G_0^*(e^{j\omega}) - G_{\theta}^*(e^{j\omega}) \\ N_0^*(e^{j\omega}) - N_{\theta}^*(e^{j\omega})\end{array}\right]\frac{1}{N_{\theta}(e^{j\omega})} + \Phi_e(e^{j\omega'}, e^{j\omega}).\end{aligned}$$

By Schur complementary factorization of

$$\left[\begin{array}{cc}\Phi_u(e^{j\omega'}, e^{j\omega}) & \Phi_{ue}(e^{j\omega'}, e^{j\omega}) \\ \Phi_{eu}(e^{j\omega'}, e^{j\omega}) & \Phi_e(e^{j\omega'}, e^{j\omega})\end{array}\right]$$

and a bias term defined as

$$B_{\theta}(e^{j\omega}) = \frac{(N_0(e^{j\omega}) - N_{\theta}(e^{j\omega}))\,\Phi_{eu}(e^{j\omega'}, e^{j\omega})}{\Phi_u(e^{j\omega'}, e^{j\omega})},$$

we obtain (see Section 8.5 in [29] for details)

$$\begin{aligned}\Phi_{\varepsilon}(e^{j\omega'}, e^{j\omega}) &= \frac{\left(G_0(e^{j\omega'}) - G_{\theta}(e^{j\omega'}) + B_{\theta}(e^{j\omega'})\right)}{N_{\theta}(e^{j\omega'})}\cdot\Phi_u(e^{j\omega'}, e^{j\omega})\cdot\frac{(G_0(e^{j\omega}) - G_{\theta}(e^{j\omega}) + B_{\theta}(e^{j\omega}))}{N_{\theta}(e^{j\omega})} \\ &\quad + \frac{\left(N_0(e^{j\omega'}) - N_{\theta}(e^{j\omega'})\right)}{N_{\theta}(e^{j\omega'})}\cdot\left[\Phi_e(e^{j\omega'}, e^{j\omega}) - \frac{\Phi_{ue}(e^{j\omega'}, e^{j\omega})\Phi_{eu}(e^{j\omega'}, e^{j\omega})}{\Phi_u(e^{j\omega'}, e^{j\omega})}\right]\cdot\frac{(N_0(e^{j\omega}) - N_{\theta}(e^{j\omega}))}{N_{\theta}(e^{j\omega})} \\ &\quad + \Phi_e(e^{j\omega'}, e^{j\omega}).\end{aligned} \tag{6.50}$$

Substituting (6.50) into (6.48) gives a generalized version of (6.3) for an LTI system with a nonstationary input. Most discussion based on (6.3) in [29] is also applicable to (6.48) and (6.50), by giving components new interpretations. If u is WSS, (6.48) simplifies to (6.3) as expected. In Section 6.3, we have shown that identifiability in the traditional direct

approach is lost due to the correlation between u_T and e_T that makes the second weighting term in (6.3) zero. On the contrary, the corresponding term in (6.50) will be shown in the next step to be nonzero, i.e.,

$$\Phi_e(e^{j\omega'}, e^{j\omega})\Phi_u(e^{j\omega'}, e^{j\omega}) - \Phi_{ue}(e^{j\omega'}, e^{j\omega})\Phi_{eu}(e^{j\omega'}, e^{j\omega}) \neq 0.$$

Step 3: Weighting Term Represented by Bispectra

Since only the spectrum of ε on the diagonal line $\omega = \omega'$ plays a role in (6.47), from (6.42), (6.43) and (6.44), the bispectrum of u on the diagonal line is

$$\Phi_u\left(e^{j\omega'}, e^{j\omega}\right) = P_u^0\left(e^{j\omega}\right) = \sum_{r=0}^{P-1} F_r\left(e^{j\omega}\right) F_r^*\left(e^{j\omega}\right) \lambda_0, \tag{6.51}$$

and the cross bispectra of u and e on the diagonal line are

$$\Phi_{ue}\left(e^{j\omega'}, e^{j\omega}\right) = F_0\left(e^{j\omega}\right)\lambda_0, \tag{6.52}$$

$$\Phi_{eu}\left(e^{j\omega'}, e^{j\omega}\right) = \lambda_0 F_0^*\left(e^{j\omega}\right), \tag{6.53}$$

where λ_0 is the power spectrum of e. From (6.51), (6.52) and (6.53),

$$\begin{aligned} & \Phi_e(e^{j\omega'}, e^{j\omega})\Phi_u(e^{j\omega'}, e^{j\omega}) - \Phi_{ue}(e^{j\omega'}, e^{j\omega})\Phi_{eu}(e^{j\omega'}, e^{j\omega}) \\ = & \left(\sum_{r=0}^{P-1} F_r\left(e^{j\omega}\right) F_r^*\left(e^{j\omega}\right) \lambda_0^2\right) - F_0\left(e^{j\omega}\right) F_0^*\left(e^{j\omega}\right) \lambda_0^2 \\ = & \sum_{r=1}^{P-1} \left|F_r\left(e^{j\omega}\right)\right|^2 \lambda_0^2. \end{aligned} \tag{6.54}$$

Equation (6.54) will be nonzero if $F_r\left(e^{j\omega}\right) \neq 0$, for $r = 1, 2, \cdots, P-1$, which is true in the fast-sampling direct approach. Therefore, identifiability is achieved.

6.8 Examples and Analysis

In this section, we apply the above theoretical results to analyze the performance of the fast-sampling direct approach. First, Example 6.3 shows the effectiveness of the approach. Second, a variation of Example 6.3 reveals a problem that motivates a further investigation. Third, we analyze the proposed approach thoroughly, and give some comments.

Example 6.3

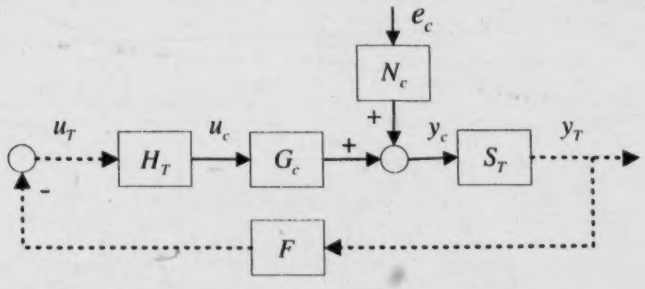

Figure 6.12: Block diagram of a closed-loop system without external excitation

Given a SISO closed-loop system without external excitation depicted in Figure 6.12 where $T = 0.4$ sec and the variance of the white noise e_c is 0.1. The true process and the noise system are

$$G_c(s) = \frac{1}{2s+1},\ N_c(s) = \frac{s+1.2}{s+0.6}.$$

The controller is $F(z) = 1$ with the control period T. To use the fast-sampling direct approach, we let $P = 2$, i.e., $h = T/P = 0.2$ sec. First, y_c is sampled with period h into y, whose sampling rate is twice faster than y_T. A fast-rate input u with period h is available from u_T because of the zero-order hold. Second, based on y and u, we estimate fast-rate models G_θ and N_θ by the PEM algorithms

$$G_\theta(z) = \frac{0.09136}{z-0.9128},\ N_\theta(z) = \frac{z-0.7782}{z-0.8765},$$

while the true fast-rate systems $G_0 := S_h G_c H_h$ and $N_0 := S_h N_c H_h$ are

$$G_0(z) = \frac{0.09516}{z-0.9048},\ N_0(z) = \frac{z-0.7738}{z-0.8869}.$$

Finally, from the fast-rate models we compute uniquely the slow-rate models with period T, whose Bode plots are shown in Figures 6.13 and 6.14. As a comparison, the models obtained by the traditional direct approach that uses the slow-rate signals y_T and u_T are presented in parallel. It is clear that if there is no external excitation, the traditional direct approach loses identifiability, while the proposed approach gives a good estimation.

The fast-sampling direct approach works very well in this example (see [40] for an example of a high-order closed-loop system simulation). However, there exists a problem that the approach sometimes may not give satisfactory results.

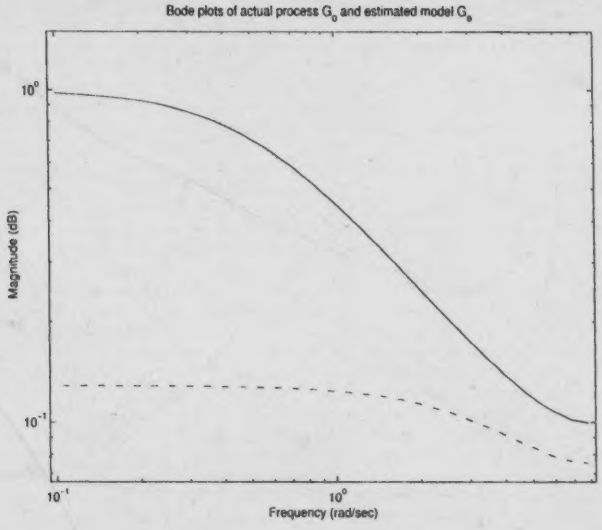

Figure 6.13: Bode plots of G_0 (solid) and G_θ obtained by the fast-sampling direct approach (dotted) and by the traditional direct approach (dashdot)

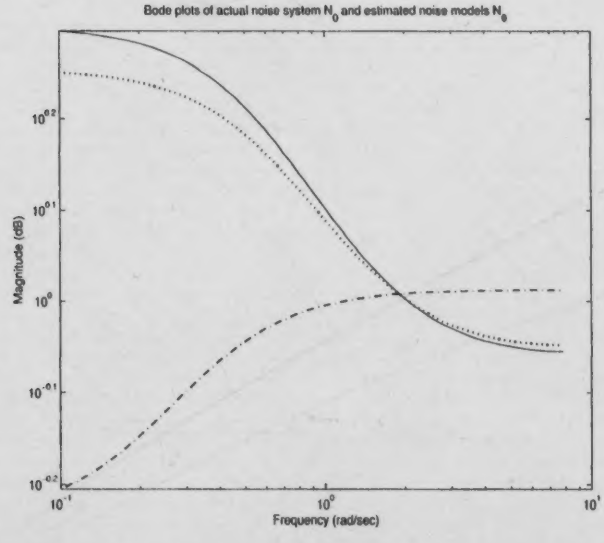

Figure 6.14: Bode plots of N_0 (solid) and N_θ obtained by the fast-sampling direct approach (dotted) and by the traditional direct approach (dashdot)

Example 6.4

We have the same configuration as that in Example 6.3 except a different controller $F(z) = 0.5$. Using the fast-sampling direct approach, we estimate models presented in Figures 6.15 and 6.16. The true dynamics are not captured well.

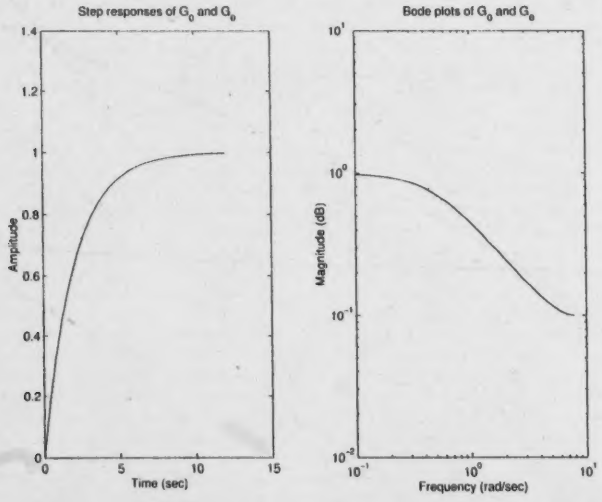

Figure 6.15: Step responses and Bode plots of G_0 (solid) and G_θ obtained by the fast-sampling direct approach (dotted)

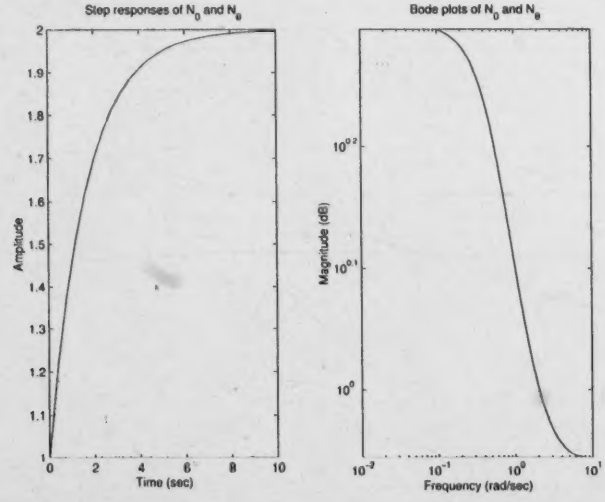

Figure 6.16: Step responses and Bode plots of N_0 (solid) and N_θ obtained by the fast-sampling direct approach (dotted)

We shall now use the bifrequency maps and bispectra to analyze the fast-sampling direct approach. The discussion is based on the frequency-domain expression (6.50), from which we see that G_θ is mainly determined by the bias term

$$B_\theta\left(e^{j\omega}\right) = \frac{\left(N_0\left(e^{j\omega}\right) - N_\theta\left(e^{j\omega}\right)\right)\Phi_{eu}(e^{j\omega'}, e^{j\omega})}{\Phi_u(e^{j\omega'}, e^{j\omega})}, \tag{6.55}$$

and N_θ is determined by the second weighting term

$$\Phi_e(e^{j\omega'}, e^{j\omega}) - \frac{\Phi_{ue}(e^{j\omega'}, e^{j\omega})\Phi_{eu}(e^{j\omega'}, e^{j\omega})}{\Phi_u(e^{j\omega'}, e^{j\omega})}. \tag{6.56}$$

We need to find these bispectra. To make the presentation easier, let us focus on the case $P = 2$. We denote the true fast-rate systems as

$$\begin{aligned} G_0 &= S_h G_c H_h := \left[\begin{array}{c|c} A_G & B_G \\ \hline C_G & D_G \end{array}\right], \\ N_0 &= S_h N_c H_h := \left[\begin{array}{c|c} A_N & B_N \\ \hline C_N & D_N \end{array}\right]. \end{aligned}$$

An $(\mathrm{LPTV})_2$ system between the fast-rate signals u and e is given in (6.15)

$$u = L_2^{-1} \underbrace{\left[-\underline{F}(I + \underline{G_0}\underline{F})^{-1}\underline{N_0}\right]}_{M} L_2 \cdot e,$$

where

$$\underline{F} = \begin{bmatrix} F & 0 \\ F & 0 \end{bmatrix}, \ \underline{G_0} = \left[\begin{array}{c|cc} A_G^2 & A_G B_G & B_G \\ \hline C_G & D_G & 0 \\ C_G A_G & C_G B_G & D_G \end{array}\right], \ \underline{N_0} = \left[\begin{array}{c|cc} A_N^2 & A_N B_N & B_N \\ \hline C_N & D_N & 0 \\ C_N A_N & C_N B_N & D_N \end{array}\right].$$

From (6.14),

$$M = \begin{bmatrix} M_0 & M_1 \\ M_0 & M_1 \end{bmatrix},$$

where

$$\begin{aligned} M_0 &= -F\left[1 + (G_{11} + G_{12})F\right]^{-1} N_{11}, \\ M_1 &= -F\left[1 + (G_{11} + G_{12})F\right]^{-1} N_{12}, \end{aligned}$$

and

$$\begin{aligned} G_{11} &= \left[\begin{array}{c|c} A_G^2 & A_G B_G \\ \hline C_G & D_G \end{array}\right], \ G_{12} = \left[\begin{array}{c|c} A_G^2 & B_G \\ \hline C_G & 0 \end{array}\right], \\ N_{11} &= \left[\begin{array}{c|c} A_N^2 & A_N B_N \\ \hline C_N & D_N \end{array}\right], \ N_{12} = \left[\begin{array}{c|c} A_N^2 & B_N \\ \hline C_N & 0 \end{array}\right]. \end{aligned}$$

Equation (6.29) shows that

$$B_0(z) = (1 + z^{-1})M_0\left(z^2\right), \ B_1(z) = (1 + z^{-1})M_1\left(z^2\right).$$

When $P = 2$, the DFT matrix is $W_2 = \begin{bmatrix} 1 & 1 \\ 1 & -1 \end{bmatrix}$. From (6.34),

$$\begin{bmatrix} A_0(z) \\ A_1(z) \end{bmatrix} = \frac{1}{2} W_2^{\dagger} \begin{bmatrix} B_0(z) \\ B_1(z) \end{bmatrix} = \frac{1}{2} \begin{bmatrix} B_0(z) + B_1(z) \\ B_0(z) - B_1(z) \end{bmatrix}.$$

With these results, the bispectra can be computed from (6.37), (6.42), (6.43) and (6.44)

$$\begin{aligned} \Phi_u(e^{j\omega'}, e^{j\omega}) &= \left|F_0\left(e^{j\omega}\right)\right|^2 \lambda_0^2 + \left|F_1\left(e^{j\omega}\right)\right|^2 \lambda_0^2, \\ \Phi_{ue}(e^{j\omega'}, e^{j\omega}) &= \lambda_0 F_0\left(e^{j\omega}\right), \ \Phi_{eu}(e^{j\omega'}, e^{j\omega}) = \lambda_0 F_0^*\left(e^{j\omega}\right), \end{aligned}$$

where

$$\begin{aligned} F_0(z) &= A_0(z) \\ &= \frac{1}{2}\left(B_0(z) + B_1(z)\right) \\ &= \frac{1+z^{-1}}{2}\left(M_0\left(z^2\right) + M_1\left(z^2\right)\right) \\ &= \frac{1+z^{-1}}{2} \cdot \frac{F\left(z^2\right) \cdot \left(N_{11}\left(z^2\right) + N_{12}\left(z^2\right)\right)}{1 + \left(G_{11}\left(z^2\right) + G_{12}\left(z^2\right)\right) \cdot F\left(z^2\right)}, \end{aligned}$$

and

$$\begin{aligned} F_1(z) &= A_1(z) \\ &= \frac{1}{2}\left(B_0(z) - B_1(z)\right) \\ &= \frac{1+z^{-1}}{2}\left(M_0\left(z^2\right) - M_1\left(z^2\right)\right) \\ &= \frac{1+z^{-1}}{2} \cdot \frac{F\left(z^2\right) \cdot \left(N_{11}\left(z^2\right) - N_{12}\left(z^2\right)\right)}{1 + \left(G_{11}\left(z^2\right) + G_{12}\left(z^2\right)\right) \cdot F\left(z^2\right)}. \end{aligned}$$

Since N_θ will affect G_θ through B_θ, let us check the second weighting term (6.56) first. From (6.51) and (6.54),

$$\Phi_e(e^{j\omega'}, e^{j\omega}) - \frac{\Phi_{ue}(e^{j\omega'}, e^{j\omega})\Phi_{eu}(e^{j\omega'}, e^{j\omega})}{\Phi_u(e^{j\omega'}, e^{j\omega})} = \frac{\sum_{r=1}^{P-1} \left|F_r\left(e^{j\omega}\right)\right|^2 \lambda_0^2}{\sum_{r=0}^{P-1} \left|F_r\left(e^{j\omega}\right)\right|^2 \lambda_0} =: W\lambda_0,$$

where

$$W = 1 - \frac{\left|F_0\left(e^{j\omega}\right)\right|^2}{\sum_{r=0}^{P-1} \left|F_r\left(e^{j\omega}\right)\right|^2}.$$

Thus, W is a real function with range $(0, 1)$. In order to get a good estimation of the noise system, we want the weighting term to be large. It is equivalent to requiring that F_0 occupies a small portion in all F_r, which is reasonable by considering a fact that only F_r for $r \neq 0$ provides information in (6.50). When $P = 2$,

$$W = 1 - \frac{\left|N_{11}\left(e^{2j\omega}\right) + N_{12}\left(e^{2j\omega}\right)\right|^2}{\left|N_{11}\left(e^{2j\omega}\right) + N_{12}\left(e^{2j\omega}\right)\right|^2 + \left|N_{11}\left(e^{2j\omega}\right) - N_{12}\left(e^{2j\omega}\right)\right|^2}. \tag{6.57}$$

Equation (6.57) reveals that W is only related to the characteristics of the noise system (The conclusion can be shown to be true in general). Therefore, we prefer a large variation between N_{11} and N_{12} in order to get a good estimation, e.g., the noise system has a small time constant.

Second, we investigate the bias term (6.55). From (6.51) and (6.53), we have

$$B_\theta\left(e^{j\omega}\right) = \left(N_0\left(e^{j\omega}\right) - N_\theta\left(e^{j\omega}\right)\right)\frac{F_0^*\left(e^{j\omega}\right)}{\sum_{r=0}^{P-1}\left|F_r\left(e^{j\omega}\right)\right|^2}. \tag{6.58}$$

When $P = 2$,

$$\begin{aligned}\left|B_\theta\left(e^{j\omega}\right)\right| &= \left|N_0\left(e^{j\omega}\right) - N_\theta\left(e^{j\omega}\right)\right|\frac{\left|F_0\left(e^{j\omega}\right)\right|}{\left|F_0\left(e^{j\omega}\right)\right|^2 + \left|F_1\left(e^{j\omega}\right)\right|^2} \\ &= \left|N_0\left(e^{j\omega}\right) - N_\theta\left(e^{j\omega}\right)\right|\frac{\left|N_{11}\left(e^{2j\omega}\right) + N_{12}\left(e^{2j\omega}\right)\right|\cdot\left|1 + \left(G_{11}\left(e^{2j\omega}\right) + G_{12}\left(e^{2j\omega}\right)\right)F\left(z^4\right)\right|}{\left|\frac{1+e^{-2j\omega}}{2}\right|\cdot\left|F\left(e^{2j\omega}\right)\right|\cdot\left(\left|N_{11}\left(e^{2j\omega}\right) + N_{12}\left(e^{2j\omega}\right)\right|^2 + \left|N_{11}\left(e^{2j\omega}\right) - N_{12}\left(e^{2j\omega}\right)\right|^2\right)}.\end{aligned} \tag{6.59}$$

Equation (6.59) reveals that B_θ is related to all the dynamics in the closed-loop system: the noise system, the process and the controller. To get a good estimation, we need the bias term to be small. Let us comment on the roles of the controller and the process, while the noise system plays the same role as that in (6.57). In (6.59), F and G_0 affect the bias distribution in a complicated way. Thus, an affirmative conclusion is hard to make. However, if F is a proportional controller, a larger gain will lower B_θ and bring a better estimation ($G_0 - G_\theta$ is small); if the time constant of G_c is too large, the estimation may be unsatisfactory.

Example 6.5

Based on Example 6.3, a set of identification results are listed here. To evaluate the size of W, we take its Euclidean norm and infinity norm. Similarly, we use $\mathcal{H}_2$-norm and $\mathcal{H}_\infty$-norm to measure the model mismatch. The results are consistent with our analysis.

	$\lvert W\rvert_2$	$\lvert W\rvert_\infty$	$\lvert G_0 - G_\theta\rvert_2$	$\lvert N_0 - N_\theta\rvert_2$	$\lvert G_0 - G_\theta\rvert_\infty$	$\lvert N_0 - N_\theta\rvert_\infty$
$G_c(s) = \frac{1}{2s+1}$ $N_c(s) = \frac{s+1.2}{s+0.6}$ $F(z) = 1$	40.6849	0.5668	0.0144	0.0589	0.0475	0.2029
$G_c(s) = \frac{1}{2s+1}$ $N_c(s) = \frac{s+0.6}{s+0.3}$ $F(z) = 1$	40.1284	0.5318	0.0465	0.0977	0.1862	0.4927
$G_c(s) = \frac{1}{4s+1}$ $N_c(s) = \frac{s+1.2}{s+0.6}$ $F(z) = 1$	40.6849	0.5668	0.0891	0.0657	0.6497	0.1938
$G_c(s) = \frac{1}{2s+1}$ $N_c(s) = \frac{s+1.2}{s+0.6}$ $F(z) = 0.5$	40.6849	0.5668	0.0955	0.0577	0.4361	0.1460

There are two other components in the closed-loop system: the variance λ_0 of the white noise and the fast-sampling ratio P. The bias term (6.58) and the weighting terms in (6.50) reveal that λ_0 has no effect on the estimation and works only as a scaling factor in (6.50). This is intuitively natural since the whole system is driven by the white noise only. There is a tradeoff in the role of P. If P increases, F_0 will occupy a smaller portion in all F_r, which makes identification towards a good direction. On the other hand, h will be smaller if P is increased. This is equivalent to increasing time constants of systems, which will deteriorate estimation results. A simulation demonstrating the effect of P is given in [40] with an implicit explanation.

Up to now, we have discussed qualitatively how the components in the closed-loop system affect the performance of the fast-sampling direct approach. The main conclusion is that applying this approach requires additional care. In other words, a satisfactory estimation sometimes may not be achieved. Indeed, this "nonideal" characteristic of the fast-sampling approach is natural for two facts. First, due to the existence of feedback that makes the closed-loop system less sensitive to changes than the open-loop system, the closed-loop data has less information [29]. Second, the absence of the external excitation essentially makes the problem of data lacking information even worse, since the whole closed-loop system is driven by noise only.

In summary, the fast-sampling direct approach has two advantages:

- External excitation is not required, which means that it could be a useful approach when the requirement of good control is stringent.
- Implementation of this approach is "easy", since the only extra effort compared to the traditional direct approach is to sample some signals faster.

Its main drawbacks are the following:

- Sometimes it may not be able to give a satisfactory estimation, superficially depending upon the dynamics of closed-loop systems and essentially being limited by the above two facts.
- Like the traditional direct approach, a good noise model is required.

Chapter 7

Conclusion

This thesis studies two different but related problems, identification of MRSD systems and identification of closed-loop systems without external excitation. To get a clear overall picture, we list the main contributions and some unsolved problems.

Main contributions:

- Uniqueness of extracting fast-rate systems from lifted systems, controllability and observability of lifted systems are studied thoroughly. They play an important role in the whole process of identification.
- Time-domain and frequency-domain approaches are proposed to compute fast-rate models. The frequency-domain approach using polyphase decomposition is shown to be a very powerful tool for the theoretical analysis.
- Many related topics, e.g., preservation of the causality constraint, identification of the noise systems, extension into MIMO cases, are discussed.
- A fast-sampling direct approach is studied in an instructive and insightful way. The proposed approach removes a traditional identifiability condition for closed-loop systems with linear output feedback, i.e., an external persistently exciting test signal is not required.
- Some gaps of bifrequency maps and bispectra are filled. These concepts are potentially powerful to analyze linear periodically time varying systems.

Unsolved problems:

- In the first part, the proposed identification approach for MRSD systems is in fact a two-step approach, from estimation of lifted systems to computation of fast-rate mod-

els. Although it is developed systematically and works well in real implementation, a few problems still exist. Namely, how to obtain the asymptotic variance of a fast-rate model or its parameters? How to reduce the estimation complexity if a nontrivial noise system needs to be estimated simultaneously? How to improve the identification efficiency for a very high dimensional lifted system? All of these are hard and even unsolvable for the two-step approach, but might be solved by a one-step approach, i.e., estimating the fast-rate system directly. Indeed, it is a constrained nonlinear optimization problem that is only partially studied in the system identification field.

An optimization problem

Given a general MRSD system satisfying some conditions such as the coprimeness condition in Proposition 1, let θ be a parameter set of the fast-rate process G_d with the base period h and the fast-rate noise system N_d with period h. The optimization problem is

$$\min_{\theta} \frac{1}{N} \sum_{t=1}^{N} \ell\left(\varepsilon_F(t,\theta)\right)$$

subject to structures of lifted systems $\underline{G_d}$ and $\underline{N_d}$, e.g., those in (2.7) and (5.4). Here N is the data length; $\ell(\cdot)$ is a scalar-valued function; ε_F is the filtered version of the prediction error ε, where ε is defined as the difference between the measured (lifted) output $\underline{y}$ and the predicted (lifted) output $\underline{\hat{y}}$ obtained from an overall lifted system

$$\underline{y} = \underline{G_d}\,\underline{u} + \underline{N_d}\,\underline{e}.$$

- In the second part, we notice that the fast-sampling direct approach may not give good estimation for some systems. To explain this, we analyze the proposed approach qualitatively. However, is it possible to give a quantitive index that is able to indicate whether the approach will work well for a given closed-loop system or a set of data?

Bibliography

[1] S. Akkarakaran and P. P. Vaidyanathan, Bifrequency and bispectrum maps: a new look at multirate systems with stochastic inputs, *IEEE Trans. Signal Processing*, **48(3)**, 723-736, 2000.

[2] K. J. Åström and B. Wittenmark, *Computer-Controlled Systems: Theory and Design*, 3rd ed. Prentice Hall, Englewood Cliffs, N.J., 1997.

[3] L. Chai and L. Qiu, Model Validation of Multirate Systems From Time-Domain Experimental Data, *IEEE Trans. Automat. Control*, **47(2)**, 346-351, 2002.

[4] T. Chen and L. Qiu, $\mathcal{H}_\infty$ design of general multirate sampled-data control system, *Automatica*, **30**, 1139-1152, 1994.

[5] T. Chen and B. A. Francis, *Optimal Sampled-data Control Systems*, Springer, London, 1995.

[6] T. Chen, Nonuniform multirate filter bank: analysis and design with an $\mathcal{H}_\infty$ performance measure, *IEEE Trans. Signal Processing*, **45(3)**, 572–582, 1997.

[7] T. A. C. M. Classen and W. F. G. MecklenbrÅker, On stationary linear time-varying systems, *IEEE Trans. Circuits Syst.*, **29(3)**, 169-184, 1982.

[8] P. Colaneri, R. Scattolini and N. Schiavoni, Stabilization of multirate sampled-data linear systems, *Automatica*, **26**, 377-380, 1990.

[9] R. E. Crochiere and L. R. Rabiner, *Multirate Digital Signal Processing*, Engelwood Cliffs, NJ: Prentice-Hall, 1983.

[10] J. H. Davis, Stability conditions derived from spectral theory: discrete system with periodic feedback, *SIAM J. Control*, **10**, 1–13, 1972.

[11] D. Doi and S. M. Phillips, Multirate identification: a multiple model parameterization, *Proc. of American Control Conf.*, 2000–2001, 1993.

[12] U. Forssell and L. Ljung, Closed-loop identification revisited, *Automatica*, **35**, 1215–1241, 1999.

[13] B./A. Francis and T. T. Georgiou, Stability theory for linear time-invariant plants with periodic digital controllers, *IEEE Trans. Automat. Control*, **33(9)**, 820–832, 1988.

[14] W. A. Gardner, *Introduction to Random Processes with Application to Signals and Systems*, 2nd ed. New York: McGraw-Hill, 1990.

[15] M. Gevers and L. Ljung, Optimal experiment designs with respect to the intended model application, *Automatica*, **22**, 543–555, 1986.

[16] R. D. Gudi, S. L. Shah and M. R. Gray, Adaptive multirate state and parameter estimation strategies with application to a bioreactor, *AIChE Journal*, **41(11)**, 2451-2464, 1995.

[17] I. Gustavsson, L. Ljung and T. Söderström, Identification of processes in closed loop – identifiability and accuracy, *Automatica*, **13**, 59–77, 1977.

[18] B. Huang and S. L. Shah, Closed-loop identification: a two-step approach, *J. Process Control*, **7(6)**, 425–438, 1997.

[19] R. E. Kalman and J. E. Bertram, A unified approach to the theory of sampling systems, *J. Franklin Inst.*, **267**, 405–436, 1959.

[20] R. E. Kalman, Y. C. Ho and K. Narendra, Controllability of linear dynamical systems, In *Contributions to Differential Equations*, **1**, Interscience, New York, 1963.

[21] P. P. Khargonekar, K. Poolla and A. Tannenbaum, Robust control of linear time-invariant plants using periodic compensation, *IEEE Trans. Automat. Control*, **AC-30**, 1088–1096, 1985.

[22] C. H. Knapp and C. Carter, Generalized correlation method for estimation of time-delay, *IEEE Trans. Acoust., Speech, Signal Processing*, **24**, 320–327, 1976.

[23] G. M. Kranc, Input-output analysis of multirate feedback systems, *IEEE Trans. Automat. Control*, **3**, 21–28, 1957.

[24] D. C. Lay, *Linear Algebra and its Application*, 2nd ed. Addison-Wesley, Reading, Mass, 2000.

[25] J. H. Lee, M. S. Gelormino and M. Morari, Model predictive control of multi-rate sampled-data systems: a state-space approach, *Int. J. Control*, **55(1)**, 153–191, 1992.

[26] D. Li, *System Identification and Control of Multirate Systems (PhD-thesis)*, University of Alberta, 2001.

[27] D. Li, S. L. Shah and T. Chen, Identification of fast-rate models from multirate data, *Int. J. Control*, **74(7)**, 680–689, 2001.

[28] D. Li, S. L. Shah, T. Chen and K. Qi, Application of dual-rate modeling to CCR octane quality inferential control, to appear in *IEEE Trans. on Control Systems Tech*, Jan. 2003.

[29] L. Ljung, *System Identification: Theory for the User*, 2nd ed. Prentice Hall, Englewood Cliffs, N. J., 1999.

[30] L. Ljung, *The System Identification Toolbox: The Manual*, 5th ed. The MathWorks Inc, Natick, MA., 2001.

[31] C. M. Loeffler and C. S. Burrus, Optimal design of periodically time-varying and multirate digital filters, *IEEE Trans. Acoust., Speech, Signal Processing*, **32(5)**, 991-997, 1984.

[32] W. Lu and D. G. Fisher, Output estimation with multirate sampling, *Int. J. Control*, **48(1)**, 149–160, 1988.

[33] W. Lu and D. G. Fisher, Least-squares output estimation with multirate sampling, *IEEE Trans. Automat. Control*, **34(6)**, 669–672, 1989.

[34] A. Papoulis, *Probability, Random Variables and Stochastic Processes*, New York: McGraw-Hill, 1965.

[35] P. Z. Peebles, *Probability, Random Variables and Random Signal Principles*, 4th ed. New York: McGraw-Hill, 2001.

[36] V. P. Sathe and P. P. Vaidyanathan, Effects of multirate systems on the statistical properties of random signals, *IEEE Trans. Signal Processing*, **41(1)**, 131-146, 1993.

[37] J. Sheng, T. Chen and S. L. Shah, Time-delay estimation of multirate systems based on interactor matrices, to appear in *Proc. of DCDIS Conf. Engineering Applications and Computational Algorithms*, Guelph, Canada, May 15-18, 2003.

[38] T. Söderström and P. Stoica, *System Identification*, Prentice Hall, International, London, 1989.

[39] L. Sun, W. Liu and A. Sano, Over-sampling approach to closed-loop identification, *Proc. IEEE CDC*, 1253–1258, 1997.

[40] L. Sun, H. Ohmori and A. Sano, Output intersampling approach to direct closed-loop identification, *IEEE Trans. Automat. Control*, **46(12)**, 1936–1941, 2001.

[41] B. Wahlberg, L. Ljung, Design variables for bias distribution in transfer function estimation, *IEEE Trans. Automat. Control*, **AC-31**, 134–144, 1986.

[42] P. P. Vaidyanathan, *Multirate Systems and Filter Banks*, Englewood Cliffs, NJ: Prentice-Hall, 1993.

[43] M. Verhaegen and X. Yu, A class of subspace model identification algorithms to identify periodically and arbitrarily time-varying systems, *Automatica*, **31(2)**, 201–216, 1994.

[44] L. A. Zadeh, Frequency analysis of variable networks, *Proc. IRE*, **38(3)**, 291–299, 1950.

Appendix A

Proposition 3 *There exists a one-to-one correspondence between* Γ *and a positive integer* k *such that* τ *is estimated as* $kh < \hat{\tau} \leq kh + h$.

Before proving it, we introduce an inequality. During one sample period mnh, say $[lmnh, (l+1)\,mnh)$, $\underline{u}_j$ is sampled at the time instant $(lmnh + jmh)$ and $\underline{y}_i$ at $(lmnh + inh)$, where l is a positive integer and $\underline{u}_j$, $\underline{y}_i$ are defined in Section 3.2. The actual time delay τ_{ij} from $\underline{u}_j$ to $\underline{y}_i$, incorporating the effect of lifting, is

$$\tau_{ij} = \tau + jmh - inh. \tag{A-1}$$

Meanwhile, τ_{ij} is estimated from l_{ij} within one sample period, i.e.,

$$(l_{ij} - 1)\,mnh < \tau_{ij} \leq l_{ij}mnh. \tag{A-2}$$

Substituting (A-1) into (A-2), we get the relation between l_{ij} and τ:

$$(l_{ij} - 1)\,mnh < \tau + jmh - inh \leq l_{ij}mnh. \tag{A-3}$$

Proof: It suffices to show that as τ varies one h interval, one and only one element in Γ will change (an idea from Sheng, *et al.* [37]). The proof consists of two parts: The first part shows the "only" term by contradiction; the second part shows there must be one element in Γ changed.

Suppose two different elements in Γ, say l_{i_1,j_1} and l_{i_2,j_2}, change as τ varies one h interval, e.g., from $kh - h < \tau_1 \leq kh$ to $kh < \tau_2 \leq kh + h$. From (A-3), we have

$$(l_{i_1,j_1} - 1)\,mnh < \tau_1 + j_1mh - i_1nh \leq l_{i_1,j_1}mnh, \tag{A-4}$$

$$l_{i_1,j_1}mnh < \tau_2 + j_1mh - i_1nh \leq (l_{i_1,j_1} + 1)\,mnh. \tag{A-5}$$

Note that the changing step cannot be larger than 1, for τ varies only h interval. Eliminating τ_1 and τ_2 in (A-4) and (A-5) gives

$$l_{i_1,j_1}mnh - kh - h < j_1mh - i_1nh < l_{i_1,j_1}mnh - kh + h.$$

Since $(j_1 m - i_1 n)$ is an integer,

$$j_1 m - i_1 n = l_{i_1,j_1} mn - k. \tag{A-6}$$

Similarly to l_{i_2,j_2},

$$j_2 m - i_2 n = l_{i_2,j_2} mn - k. \tag{A-7}$$

Equations (A-6) and (A-7) give

$$(j_2 - j_1) = (l_{i_2,j_2} - l_{i_1,j_1})\, n - \frac{(i_1 - i_2)\, n}{m}.$$

Since m, n are coprime and $|j_2 - j_1| < n - 1$, we conclude $i_1 = i_2$ and $j_2 = j_1$, which causes a conflict.

Now the second part, let τ varies as:

$$\begin{aligned} kmnh \;&<\; \tau_1 \le kmnh + h, && \text{(A-8)} \\ &\vdots \\ (k+1)\, mnh \;&<\; \tau_{mn+1} \le (k+1)\, mnh + h. && \text{(A-9)} \end{aligned}$$

Define $\Delta := jmh - inh$. From (A-3), we assume

$$(l_{ij} - 1)\, mnh < \tau_1 + \Delta \le l_{ij} mnh. \tag{A-10}$$

Equations (A-8) and (A-10) imply

$$(l_{ij} - 1 - k)\, mnh \le \Delta \le (l_{ij} - k)\, mnh - h, \tag{A-11}$$

for Δ is an integer multiple of h. Thus, (A-9) and (A-11) give

$$l_{ij} mnh < \tau_{mn+1} + \Delta \le (l_{ij} + 1)\, mnh. \tag{A-12}$$

Equation (A-12) means that every element in Γ increases by one after mnh intervals, which implies that there must be one and only one element in Γ changing as τ varies one h interval, considering the proved first part. The proposition then follows. □

Appendix B

This appendix serves to prove (6.43) and (6.44). It is similar to the proof of (6.42) in [1]. Let x and y be, respectively, the input and output of an $(\mathrm{LPTV})_P$ system with Green's function $k(m,n)$. Hence, (6.22) and (6.24) are satisfied. Using (6.22), we have

$$\begin{aligned} R_{yx}(m,n) &= E\left[y(m)\,x^{\dagger}(n)\right] \\ &= E\left[\sum_{r=-\infty}^{\infty} k(m,r)\,x(r)\,x^{\dagger}(n)\right] \\ &= \sum_{r=-\infty}^{\infty} k(m,r)\,E\left[x(r)\,x^{\dagger}(n)\right] \\ &= \sum_{r=-\infty}^{\infty} k(m,r)\,R_x(r,n). \end{aligned} \tag{B-1}$$

By comparing with (6.25), (B-1) is the Green's function of the cascade of two systems with Green's functions $R_x(m,n)$ and $k(m,n)$ in this order. From (6.26), we have

$$\begin{aligned} \Phi_{yx}\left(e^{j\omega'}, e^{j\omega}\right) &= \int_{-\pi}^{\pi} K\left(e^{j\omega'}, e^{j\omega''}\right)\Phi_x\left(e^{j\omega''}, e^{j\omega}\right)\mathrm{d}\omega'' \\ &= \int_{-\pi}^{\pi} F\left(e^{j\omega'}, e^{j\omega''}\right)\left(\sum_{q=-\infty}^{\infty}\delta\left(\omega''-\omega'+\frac{2\pi q}{P}\right)\right)\Phi_x\left(e^{j\omega''}, e^{j\omega}\right)\mathrm{d}\omega'' \\ &= \sum_{q=0}^{P-1} F\left(e^{j\omega'}, e^{j\left(\omega'-\frac{2\pi q}{P}\right)}\right)\Phi_x\left(e^{j\left(\omega'-\frac{2\pi q}{P}\right)}, e^{j\omega}\right) \\ &= \sum_{q=0}^{P-1} F_q\left(e^{j\omega}\right)\Phi_x\left(e^{j\left(\omega'-\frac{2\pi q}{P}\right)}, e^{j\omega}\right), \end{aligned}$$

where the second equality follows from (6.35); the third equality uses the sifting property of the $\delta(\cdot)$ function; the last equality is the definition in (6.36).

Equation (6.44) can be proven in the same way. Using (6.22), we have

$$\begin{aligned} R_{xy}(m,n) &= E\left[x(m)\,y^{\dagger}(n)\right] \\ &= E\left\{x(m)\left[\sum_{r=-\infty}^{\infty} k(n,r)\,x(r)\right]^{\dagger}\right\} \end{aligned}$$

$$= \sum_{r=-\infty}^{\infty} E\left[x(m)\, x^{\dagger}(r)\right] k^{\dagger}(n,r)$$
$$= \sum_{r=-\infty}^{\infty} R_x(m,r)\, k^{\dagger}(n,r).$$

With a similar statement as that beneath (B-1), from (6.26), (6.35) and the sifting property of the $\delta(\cdot)$ function, we have

$$\begin{aligned}
\Phi_{xy}\left(e^{j\omega'}, e^{j\omega}\right) &= \int_{-\pi}^{\pi} \Phi_x\left(e^{j\omega'}, e^{j\omega''}\right) K^{\dagger}\left(e^{j\omega}, e^{j\omega''}\right) d\omega'' \\
&= \int_{-\pi}^{\pi} \Phi_x\left(e^{j\omega'}, e^{j\omega''}\right) F^{*}\left(e^{j\omega}, e^{j\omega''}\right) \sum_{q=-\infty}^{\infty} \delta\left(\omega'' - \omega + \frac{2\pi q}{P}\right) d\omega'' \\
&= \sum_{q=0}^{P-1} \Phi_x\left(e^{j\omega'}, e^{j\left(\omega - \frac{2\pi q}{P}\right)}\right) F^{*}\left(e^{j\omega}, e^{j\left(\omega - \frac{2\pi q}{P}\right)}\right) \\
&= \sum_{q=0}^{P-1} \Phi_x\left(e^{j\omega'}, e^{j\left(\omega - \frac{2\pi q}{P}\right)}\right) F^{*}\left(e^{j\omega}, e^{j\left(\omega - \frac{2\pi q}{P}\right)}\right).
\end{aligned}$$

□